NASA CP-2004

SUPPLEMENT

ATMOSPHERIC AEROSOLS:

THEIR OPTICAL PROPERTIES AND EFFECTS

A Topical Meeting on Atmospheric Aerosols

Sponsored by

Optical Society of America

and the

NASA Langley Research Center

Williamsburg, Virginia
December 13-15, 1976

NASA
National
Aeronautics and
Space
Administration

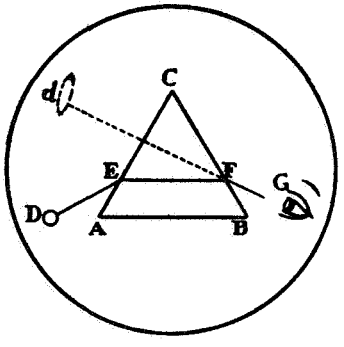

Optical Society of Americ

NASA Conference Publications (CP Series) contain compilations of scientific and technical papers or transcripts arising from conferences, workshops, symposia, seminars, and other professional meetings that NASA elects to publish.

The text of these proceedings was reproduced directly from author-supplied manuscripts for publication and distribution prior to opening of the meeting. NASA has performed no editorial review of the papers.

ASA CP-2004

SUPPLEMENT

ATMOSPHERIC AEROSOLS:
THEIR OPTICAL PROPERTIES AND EFFECTS

A digest of technical papers presented at the topical meeting on Atmospheric Aerosols: Their Optical Properties and Effects, December 13-15, 1976, Williamsburg, Virginia

Sponsored by

Optical Society of America
2000 L Street, N.W., Washington, D.C. 20036

NASA Langley Research Center
Hampton, Virginia 23665

NASA
National
Aeronautics and
Space
Administration

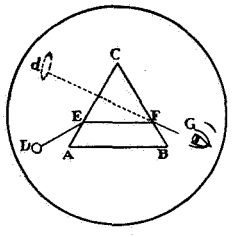

Optical Society of America

TECHNICAL PROGRAM COMMITTEE

Franklin S. Harris, Jr.,
NASA Langley Research Center
Hampton, Virginia 23665

Adarsh Deepak
NASA Langley Research Center
Hampton, Virginia 23665

Benjamin M. Herman
University of Arizona
Tucson, Arizona 85721

James D. Lawrence, Jr.
NASA Langley Research Center
Hampton, Virginia 23665

Dale A. Lundgren
University of Florida
Gainesville, Florida 32611

M. Patrick McCormick
NASA Langley Research Center
Hampton, Virginia 23665

QUENZEL, H.,[1] HEINTZENBERG, J.[2] and KOEPKE, P.[1]
[1]Meteorologisches Institut der Universitaet
Theresienstraße 37, D-8000 Muenchen 2, FRG
[2]Institut fuer Meteorologie der Universitaet
Postfach 3980, D-6500 Mainz, FRG

Aerosol Size Distribution Inverted from Spectral Solar Attenuation plus Scattering Measurements

Inversion method

The inversion technique is a least-square-method to fit measured optical data by optical data calculated from columnar aerosol size distributions via Mie theory. Starting with a single randomly selected column, its particle concentration is chosen to fit the measured data best. At the next step a second randomly selected column is added to the first column and the particle concentrations of both columns are chosen to fit the measured data best. In each of the next steps one more randomly selected column is added or its particle concentration is changed together with a joint change of all other columns to improve the best fit. The program is not time consuming because at each iteration step the least-square-equation is solved analytically. The number of columns which are allowed to contribute to the size distribution, and the size range of each column has to be chosen before the iteration is started.

Test with simulated spectral data

Unfortunately not only one columnar size distribution but a large variety of such distributions will fit the measured data. For testing the 'uniqueness' of the inversion of spectral data to size distributions, simulated spectral data have been used, calculated via Mie theory from given aerosol size distributions (including fixed refractive index). From these tests it has been found, that the information content of the extinction coefficients (optical depth) between 0.4 μm and 1.2 μm only, is insufficient with respect to realistic atmospheric aerosol size distributions. But if the information content of the scattering function especially at small scattering angles is added, the inverted size distribution agrees very well with the original size distribution. Figures 1 and 2 give for example the linear number distributions versus the particle radius, with the straight lines being the given test size distributions of the simulated spectral data. They consist of extinction coefficients at λ = 0.475, 0.605, 0.743, 0.862, 1.020, 1.650 μm and of the scattering function at the scattering angles 2°, 6°, 10°, 14°, 18° for λ = 0.605 μm. The columns give 10 distributions resulting from 10 inversions. The 10 results are obtained from different random sequences of the columns during the iteration procedure. The figures show that the variability of the inverted

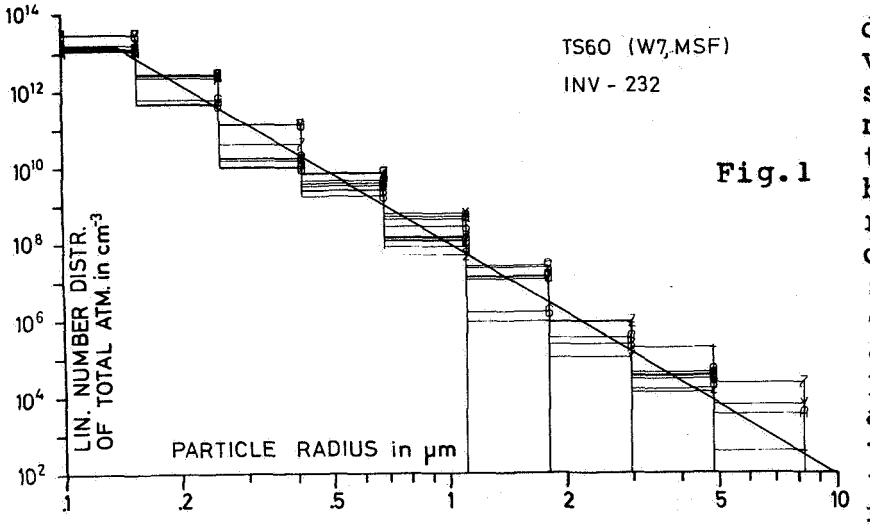

Fig.1

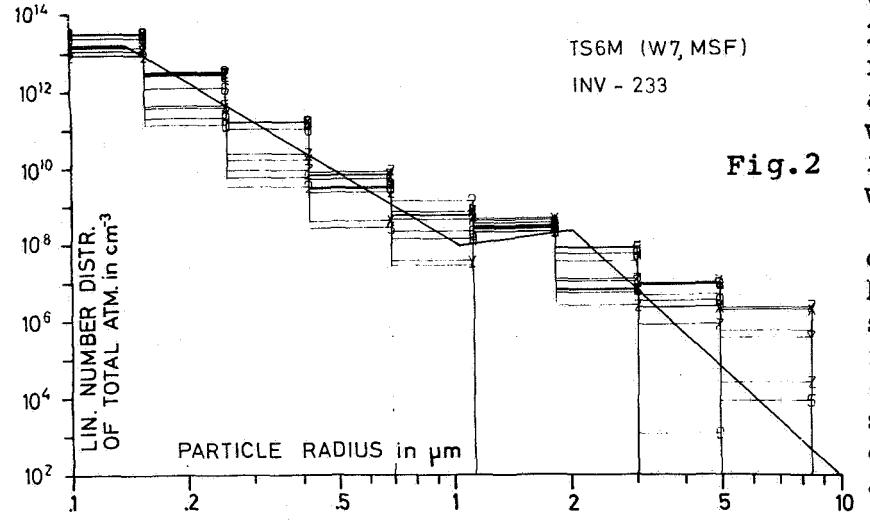

Fig.2

distributions is not very high, but one single inversion will not sufficiently meet the given size distribution. Only the averages of the resulting distributions represent both given size distributions (with and without 2 µm-peak) very well. The average of the resulting size distributions is independent from the number of inversions when at least 20 inversions are averaged. Further, the average is the same when the least-square-iteration is started with an arbitrary column or with any other distribution. This behaviour of the inversion procedure justifies the application of the method to measured data of spectral extinction coefficients and scattering functions.

Sensitivity to errors of the spectral data

The sensitivity of the resulting aerosol size distributions to measuring errors has been tested by introducing errors into the simulated spectral data of the two test distributions presented in figs. 1 and 2. If the simulated data of the test distributions are affected with statistical errors of ± 10%, the resulting size distributions are not remarkably different from that inverted from the accurate data. If the errors are higher than ± 20% the resulting size distributions are wrong with some of the columns becoming to high or to low what may be interpreted as holes or peaks.
The inversion method requires knowledge of the actual value of the real and the imaginary part of the refractive index of the aerosol particles. An extensive test about the limits inbetween which an inaccuracy of the refractive index can be accepted is not yet made. But it can be said: If the true refractive index of the test distributions is 1.50 - 0.02·i and the inversion is made under the assumption, that the refractive index is 1.33 - 0·i, the resulting

size distribution is wrong with fictitious holes and peaks. If the inversion is made under the assumption of a refractive index 1.50 - 0·i, i.e., with only the imaginary part being incorrect, the resulting size distribution is more similar to the given distribution but somewhat to inaccurate.

Application to measured data of spectral optical depth and scattering function

Our inversion procedure has been applied to measured data. From mid July to mid August 1971 ground based spectral measurements of the direct solar radiation and of the sky radiance at different points in the vicinity of the sun have been carried out in a savannah in the Southwest of Africa near Tsumeb in the dry season. From this, reliable values of the aerosol optical depth of the atmosphere have been derived at λ = 0.465, 0.605 0.8605 and 1.25 µm and values of the aerosol scattering function at the scattering angles 2^o, 6^o, 10^o, 14^o, 18^o for λ=0.605 µm and λ = 0.8605 µm. Remainig gaseous absorption at the wavelengths used has been taken into account. By means of a multiple-scattering-program the contribution of multiple scattered photons to the sky radiance has been taken into account, too. In figs.3 and 4 the resulting aerosol size distributions of four and six consecutive days are presented. The exponent x at the ordinate scale has the value 5 at 28 July, 8 at 29 July, 11 at 30 July, 14 at 31 July, 5 at 5 Aug., 8 at 6 Aug., 11 at 8 Aug., 14 at 9 Aug., 17 at 10 Aug. and 20 at 11 Aug. The straight lines are power law distributions with a Junge exponent of 3.3. They are added only to demonstrate the deviations of the real size distributions from the power law distribution.

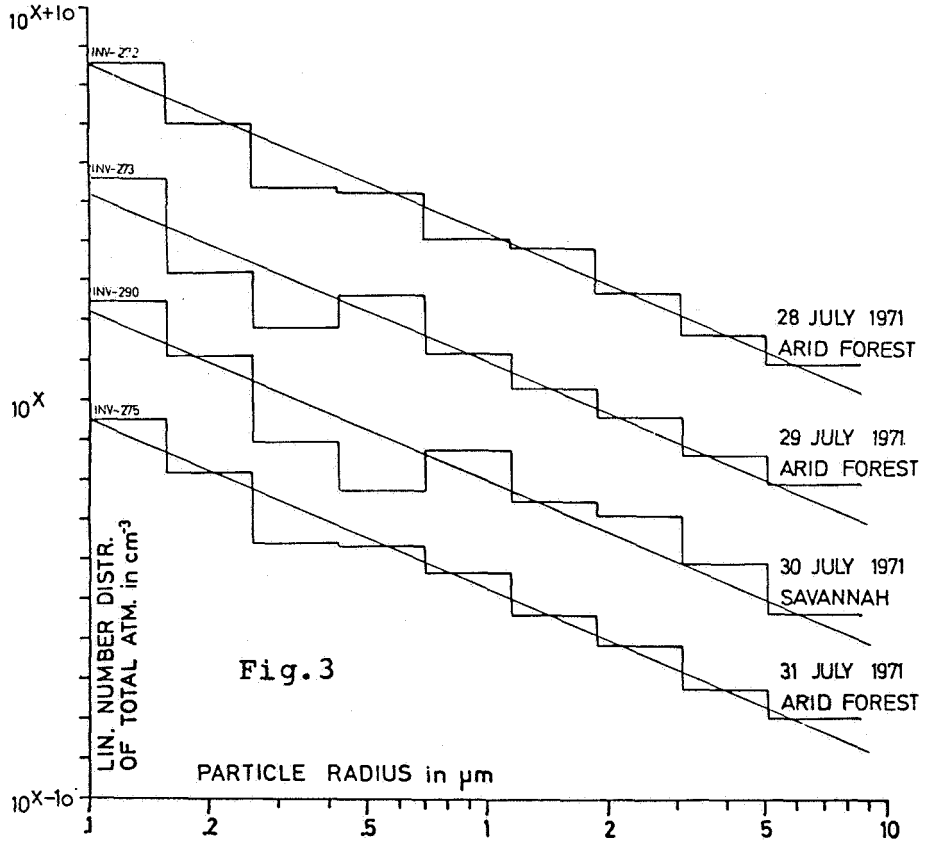

Fig.3

The respective types of earth surfaces which had been passed by the air masses in the last 3 to 4 days prior to measurement, indicated

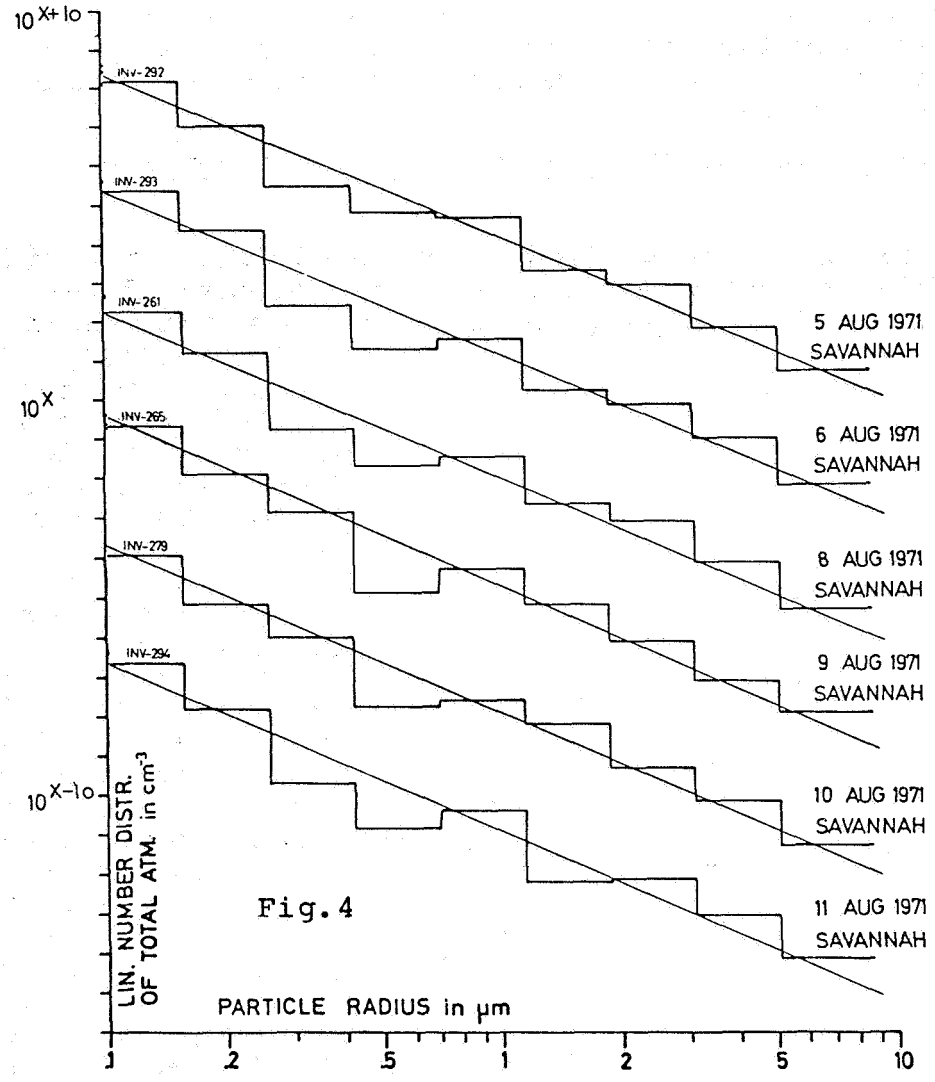

Fig. 4

on the right sides of the size distributions, are known because the trajectories of the air masses have been constructed. As to be seen from the figures, two types of aerosol size distributions have been found, correlated to the history of the air masses. The 'arid forest'-type has a peak at about 0.6 µm particle radius and the 'savannah' type has a peak at about 0.9 µm particle radius. Both types of aerosol size distributions are without any doubt bimodal distributions. The similarity of the different size distributions of each type is - for our opinion - surprisingly high.

Comparison of Extinction and Backscattering Coefficients for Measured and Analytic Stratospheric Aerosol Size Distributions

Thomas J. Swissler, Systems and Applied Sciences, Riverside, Maryland 20840
Franklin S. Harris, Jr., Old Dominion University, Norfolk, Virginia 23508

Theoretical Mie calculations for extinction and backscattering coefficients have been performed for the analytic size distributions for stratospheric aerosols at 20 km described previously by Harris and Rosen (1976). The computations were performed under the assumption of spherical particles and a single refractive index characterizing the composition of the aerosols in the stratospheric layer. Several representative indices were chosen for these calculations and the wavelengths considered for examination were those associated with ruby and neodymium lidar systems. The ruby laser wavelength of 0.6942 μm and its second harmonic 0.3472 μm as well as the neodymium laser wavelength 1.06 μm and its second harmonic 0.53 μm were utilized. Simulations of aerosol extinction and backscattering at these wavelengths were performed for use in the interpretation of satellite measurements. The ratio of aerosol extinction to backscattering may be sensitive to aerosol size distribution or to aerosol composition. This study examines the range of sensitivities of the theoretically calculated extinction and backscattering coefficients for several proposed stratospheric aerosol size distributions and for several refractive indices.

The analytic models used to describe the stratospheric aerosol size distribution have been discussed by Harris and Rosen and these models appear representative of experimental aerosol measurements observed during periods of quiescent volcanic activity. These distributions are plotted in Figure 1 in the form dN/dr, the aerosol number density per unit interval of radius r. The particle sizes considered in this study ranged from 0.02 μm to 5.00 μm radius. The data on the experimental distributions presented by Harris and Rosen indicate that there are very few stratospheric aerosols outside of this size range. The power-law size distribution was further limited to the size range 0.10 to 0.50 μm. Outside of these limits the predicted power-law distribution is not consistent with the experimental data. The total number of particles observed between the limits r_1 and r_2 is

$$N(r_1, r_2) = \int_{r_1}^{r_2} n(r)\, dr$$

where n(r) can also be described by

$$n(r) = N_o\, g(r)$$

with the normalization constant N_o, consistent with the total number of particles. This constant has been chosen such that the number of particles with radii greater than 0.15 μm is equal to 1 particle cm^{-3}. These size distributions are used with the Mie theoretical scattering terms for single particle scattering to define the aerosol extinction coefficient, β_λ and the aerosol backscattering coefficient f(180°).

$$\beta_\lambda = \pi N_o \int_{r_1}^{r_2} r^2 Q_e(2\pi r/\lambda)\, g(r)\, dr$$

where Q_e = Mie efficiency factor for extinction

λ = wavelength (in μm)

and

$$f(180°) = (N_o/k^2)\int_{r_1}^{r_2} i(m, 2\pi r/\lambda, 180°)\, g(r)\, dr$$

where $i(m, 2\pi r/\lambda, 180°)$ = Mie intensity function

$k = 2\pi/\lambda$

m = complex refractive index.

The Mie scattering terms in the above integrals were calculated using an increment in the size parameter x (where $x = 2\pi r/\lambda$) of 0.10. Values for the aerosol extinction coefficients as a function of wavelength indicate insensitivity to variation in model size distributions with the exception of the aged volcanic model with its high concentration of small size particles. There is slight variation between models for particle refractive index changes. Calculated values for the backscattering coefficient as a function of wavelength also indicate relatively little change between particle size distributions with a somewhat stronger dependence on particle refractive index.

If the ratio is taken of the extinction and backscattering coefficients a quantity is defined that is independent of the normalization used for the particular size distribution but still dependent on the shape of the distribution. Plots of the extinction to backscattering ratio as a function of wavelength are presented in Figure 2 for the aerosol composed of 75 % H_2SO_4 and 25 % H_2O and in Figure 3 for aerosol having a refractive index of 1.50 for the real part and 0.00 for the imaginary part. Better discrimination is seen in these ratio plots between the particle size distributions than is observed in calculations for either the extinction or the backscattering versus wavelength. For example the log normal model is distinct from the aged particle model, haze H and the power-law distributions. Both the haze H and background models have similar results because they are similar models.

Apparently particle composition, as shown by the effect of refractive index, can not easily be differentiated under any of the conditions considered in these calculations. However as shown in Figures 2 and 3 there is appreciable variation in the extinction to backscattering ratio with particle size distribution, which is also wavelength dependent.

Reference:

Harris, Franklin S., Jr. and James M. Rosen, (1976): Measured and analytic distributions of stratospheric aerosols: a review and commentary. Atmospheric Aerosols, Their Optical Properties and Effects, NASA CP-2004, pp. MA2-1 to 4.

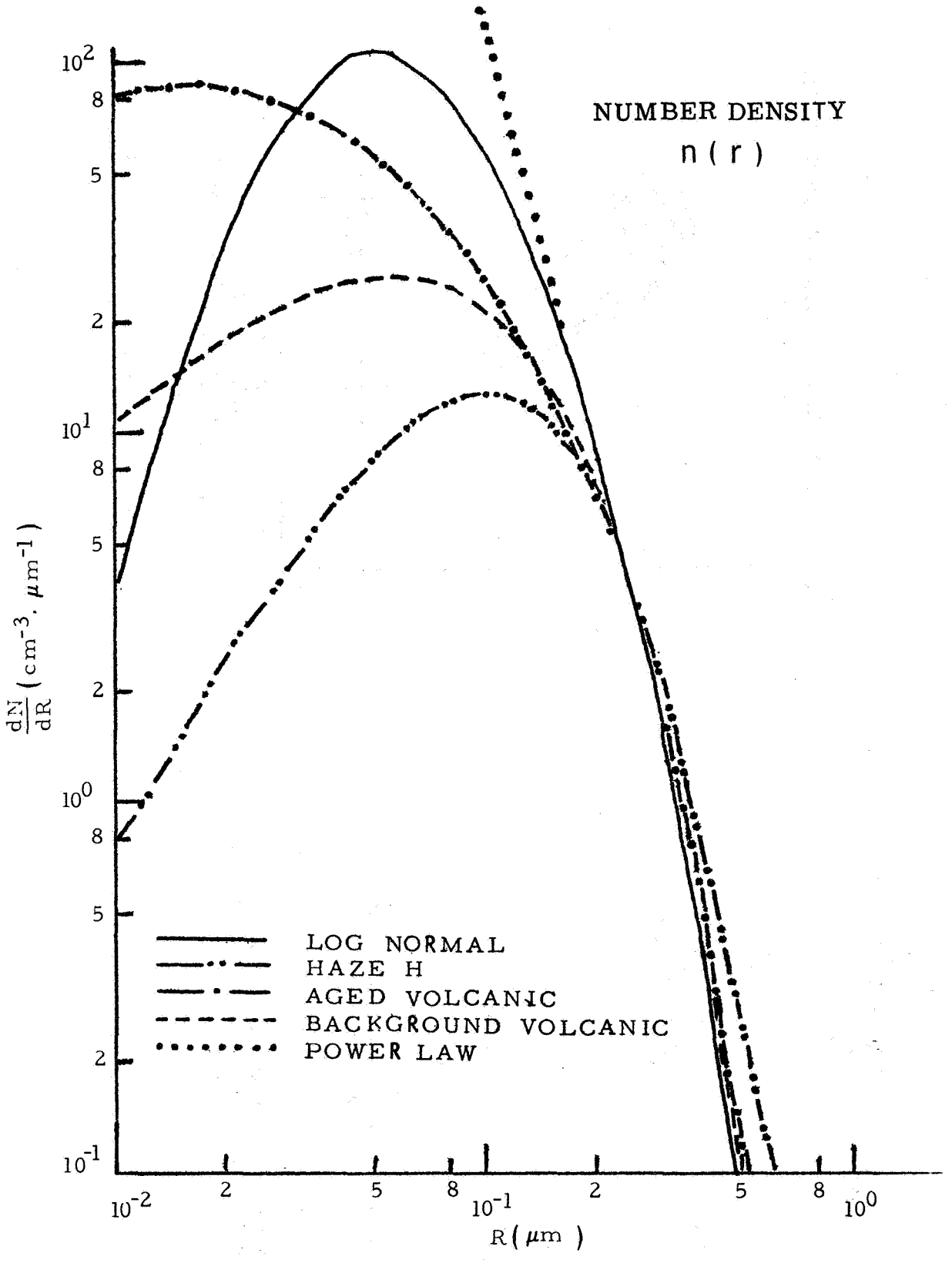

Figure 1. Stratospheric size distributions at 20 km.

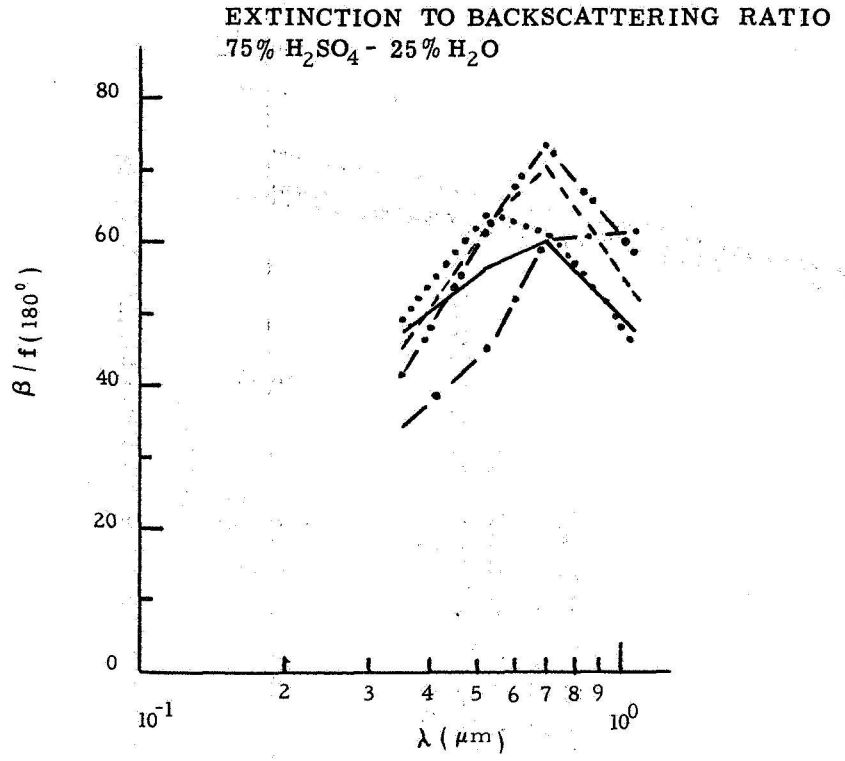

Figure 2. Spectral dependence of extinction to backscattering ratio (75% H_2SO_4 - 25% H_2O)

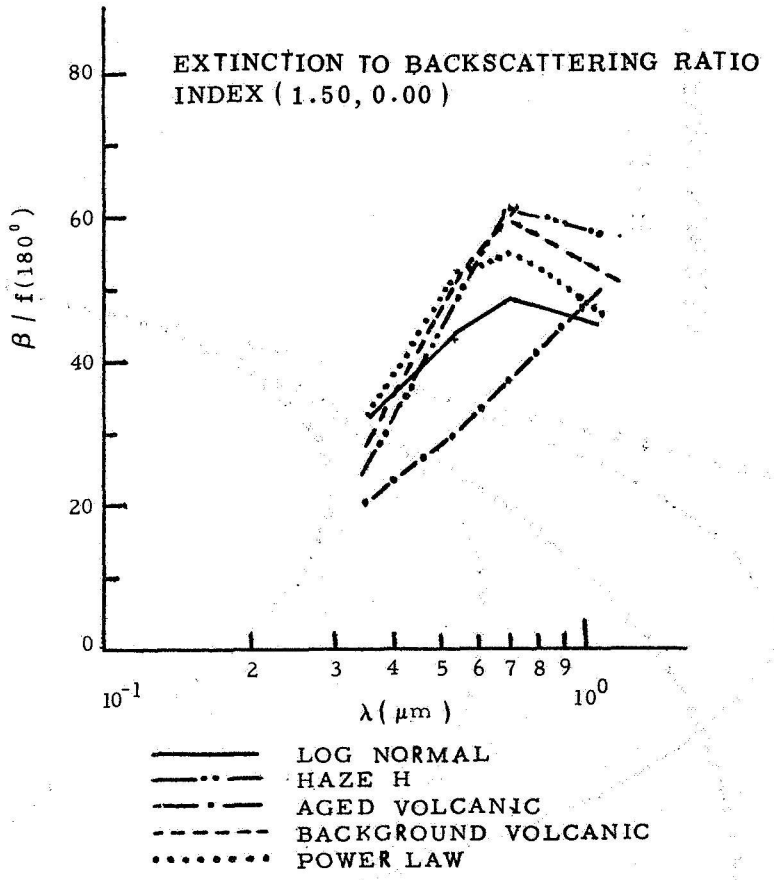

Figure 3. Spectral dependence of extinction to backscattering ratio (1.50, 0.00)

MCLL-4

KOEPKE, P. and QUENZEL, H.
Meteorologisches Institut der Universität
Theresienstrasse 37, D - 8000 München 2, FRG

Remote Sensing of Atmospheric Turbidity from Geosynchronous Orbit

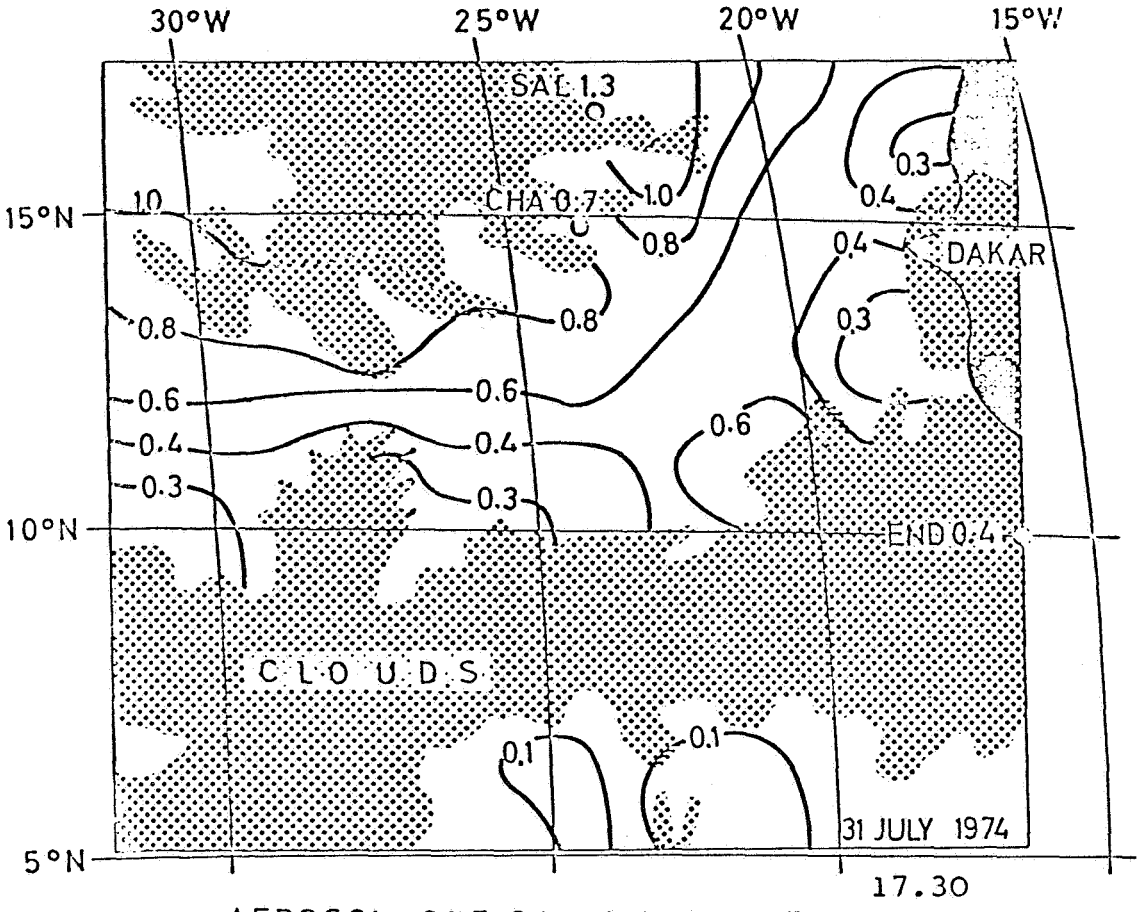

AEROSOL OPTICAL DEPTH AT 0.7 µm

Version 1.12.76

Ground truth data: 30 July 74 after Prospero et al.(1976)

SAL = Sal, Cap Verde
CHA = US Ship Charterer
END = US Ship Endurer

Literature

Prospero,J.M.,Carlson,T.N.,Savoie,D. and Nees,R.T.(1976), Technical Report, Univ. of Miami

HYBRID METHODS ARE HELPFUL

H.C.van de Hulst
Leiden Netherlands

1. Introduction

Methods to solve problems in radiative transfer and in multiple scattering exist in such a wide variety that I shall not attempt another review. In any practical problem the method must be chosen on the basis of expedience, and this in turn depends on many factors, such as :

range of variables

desired accuracy of results

occasional or frequent computations needed

cost, available funds

experience and taste

I emphasize in this talk the fact that in many situations a hybrid approach containing elements from different methods, though not "elegant", is the most practical. A normal rose or fruit tree consists of different varieties skillfully grown together because the desired properties of roots and fruits (or flowers) are not met in a single variety. The following examples may illustrate such hybrid methods.

2. The X- and Y-functions

Hybrid approaches already are helpful in the theoretical derivation, i.e., in the process that leads to a solution in analytical form. The well-known X- and Y-functions for isotropic scattering

form a good illustration. They were introduced by Ambartsumian in the early forties and extensively studied by Chandrasekhar about 1945, who defined them as solutions of certain simultaneous non-linear integral equations. Somewhat later I rediscovered the physical definition as what I would now call simple examples of point-direction gain functions and was quite pleased to find that certain properties of these functions can be far more easily derived from these physical definitions. Since that time I do not hesitate to use the two approaches mixed. What happens here is that we discover (Fig. 1) that a derivation in mathematical physics is like a suburban train. Getting on at an intermediate stop, or getting off at an intermediate stop, is equally authentic as taking the full ride and the gains in rapidity or in clarity may be considerable.

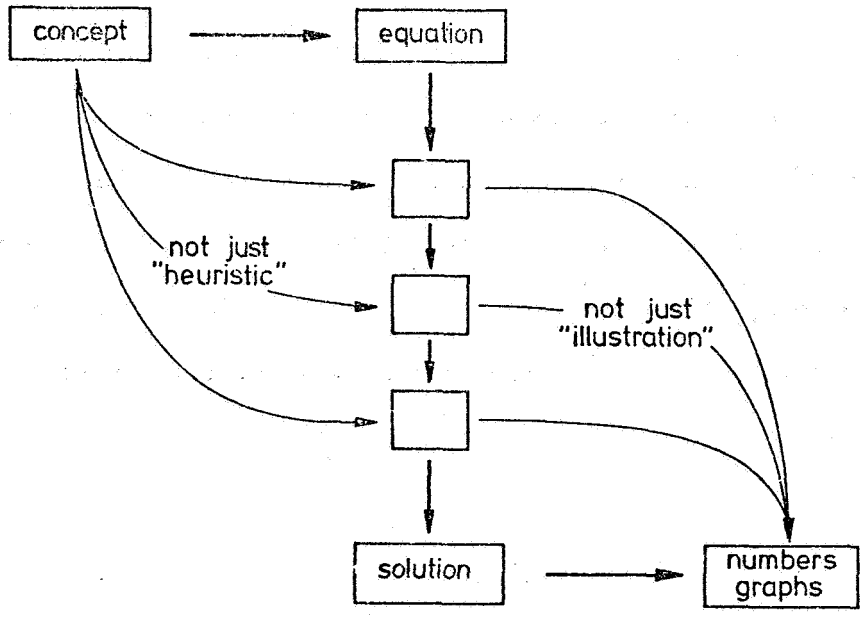

Fig. 1 In a derivation in mathematical physics access from physical concepts to intermediate stops, if done carefully, is often advisable. Likewise interpretation of intermediate numerical results may be equally important as interpretation of final numbers.

Phase functions of arbitrary form, or phase matrices with polarization, require a far more elaborate set of formulae, but the situation is basically the same : carefully preparing the access at intermediate stations pays off well.

3. Asymptotic fitting

A good example of a hybrid computational method is the method of asymptotic fitting, described elsewhere in detail. The idea is that by the doubling method we can in 10 steps bridge the range of optical thickness b = 1/32, 1/16, 1/8, ..., 8, 16, 32, but that it is silly to try to carry this process to $b = \infty$, which we can never reach. Instead, we wish to use the known asymptotic forms of the reflection and transmission functions for sufficiently large b. The process by which the different approach (asymptotic theory) is grafted onto the numerical computation (doubling) is called asymptotic fitting. It uses the doubling results of 3 successive steps, say b = 8, 16 and 32, and yields all desired functions and constants for a semi-infinite medium.

4. The corner of small losses

In the problem of reflection and transmission by a homogeneous slab of scattering particles, I like to imagine the results displayed in a diagram of a, the albedo for single scattering, against b, the optical thickness of the slab. At one corner, defined by $a = 1$, $b = \infty$, the reflection is complete. Small losses by escape from the bottom of the slab occur if b is not quite ∞ . These losses are not additive and their combined behaviour has posed nasty problems in many papers, numerical

and analytical alike. Yet the situation is simple. Both these losses have the same dependence on angle of incidence and escape because they both occur in deep layers. They add in a way which is universal, except for scale factors, and which is shown in a particular example in Figure 2.

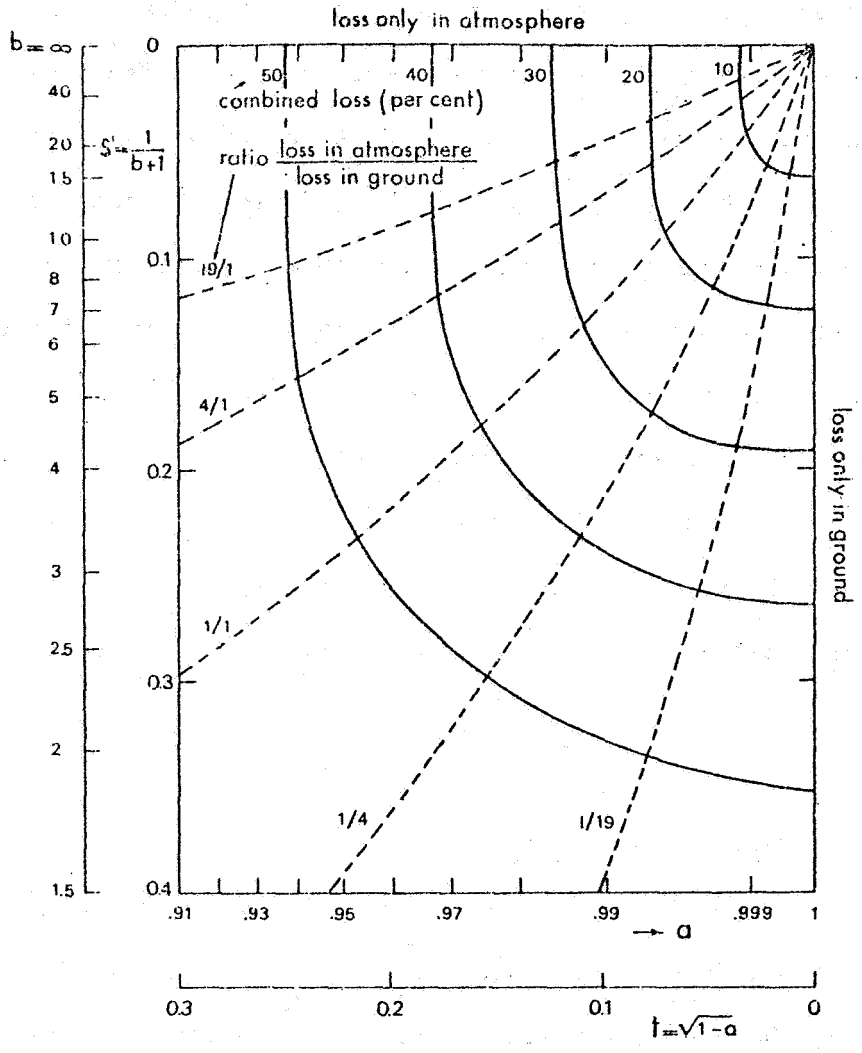

Fig. 2 Heavy curves give the combined loss = non-reflected fraction of incident flux for a finite atmosphere of thickness b consisting of isotropically scattering particles with single scattering albedo a exposed to vertically incident radiation. The curves near the lossless corner have a universal form independent of the phase function.

5. Polarization in high-order scattering

The fine visual observations of polarization of the planet Venus at various phase angles published in Lyot's thesis in 1929 have outlasted 40 years before the first tentative interpretation could be replaced by a more definite one. Lyot conjectured that polarization might be completely absent in all but first-order scattering. This guess is not correct. I took a practicing example based on Rayleigh scattering in a semi-infinite atmosphere and radiation incident under 60^{o} from the normal and reflected back to the source (as for a planet in opposition). The degree of polarization is 0 per cent in the first order, 9 per cent in the second order, and surprisingly goes up even further to 13 and 14 per cent in the third and fourth orders before it settles to 2.2 per cent in very high orders. This effect also shows up as a maximum polarization of 6.1 per cent for single scattering albedo a = 0.95. The simplest way to collect these results is to combine data obtained by very different methods.

6. Photon path distributions

The understanding of many problems, for instance, the formation of planetary absorption lines, is greatly aided by a clear knowledge of the photon path distributions. It is well known that such distributions may be obtained by an inverse Laplace transform from the dependence of the reflection function on a (albedo for single scattering). This knowledge may be put to use in various ways : the inverse Laplace transform may be applied to any form in which the reflection function is known, analytic, numerical, or asymptotic. A systematic exploration

of this possibility has made it possible to combine smoothly the results for very low orders, where ad-hoc calculations are fast, with those of high orders, where an asymptotic approach is more appropriate. An example is shown in Figure 3.

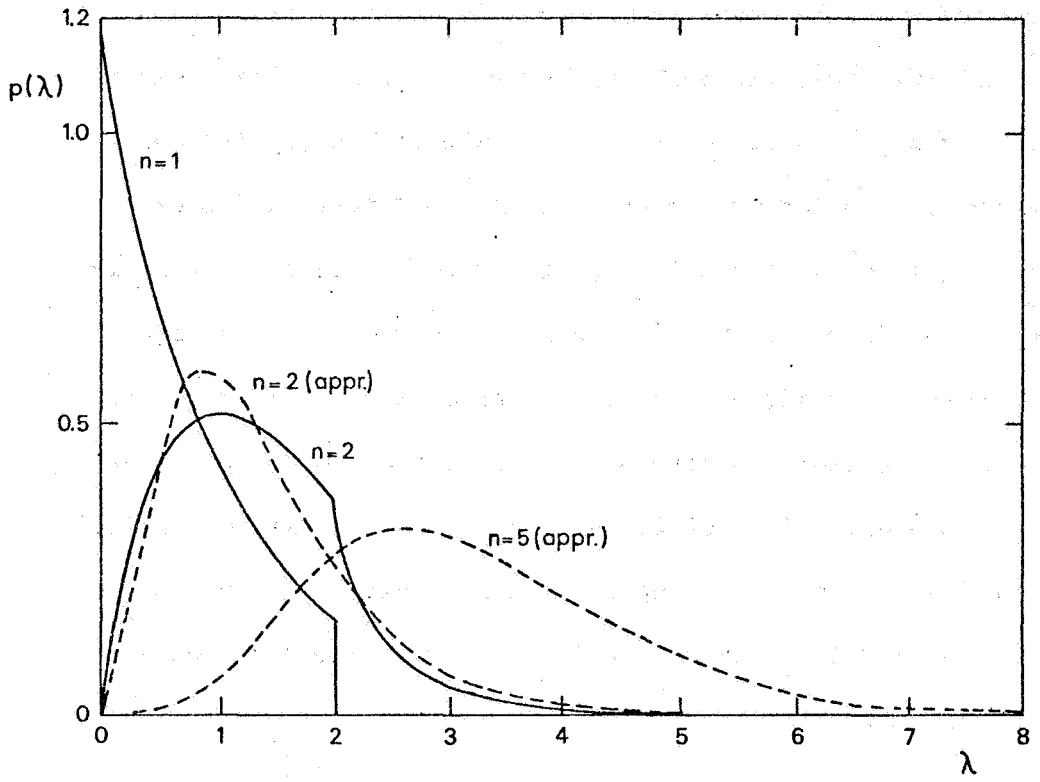

Fig. 3 Path-length distribution of radiation diffusely reflected back in vertical direction after n scattering events from a slab of isotropically scattering particles of optical thickness 1 exposed to vertical illumination. The exact forms, known for small n, rapidly approach an asymptotic theory.

References

These examples have been selected from

H.C.van de Hulst, Multiple light scattering in cloud layers, Academic Press, New York (in preparation),

where further references may be found.

"BLUE MOON", 1975

Raymond L. Chuan
Brunswick Corporation
Costa Mesa, California

The phenomenon of the blue moon, as was observed after the eruption of Krakatoa in 1883 and the extensive forest fires in Canada in 1950, had long been thought to be related to the anomalous extinction of light by atmospheric aerosols dominated by those formed by these cataclysmic events. Porch, et al[1], concluded that certain physical characteristics of atmospheric aerosols, when falling in prescribed ranges, could lead to anomalous scattering and the "blue moon" phenomenon. These conditions are, (1) the geometric standard deviation of a log-normally distributed aerosol must be ≤ 1.5, (2) the imaginary part of the refractive index of the aerosol must be ≤ 0.01, and (3) the number mean radius of the aerosols must lie in the range 0.4 to 0.9 μm. During a large brush fire in Southern California in November, 1975, with a resulting smoke cloud over most of the air basin for three days, automobile headlights were observed to be bluish (rather than reddish as might be expected in a smoke-filled atmosphere), especially when viewed through the rear-view mirror in a car on the freeway (suggesting a forward-scattering mechanism at play). With the aid of a 10-stage cascade impactor capable of generating real-time in-situ data on aerosol mass distribution by size from 0.05 to 25 μm, a number of aerosol size distributions were measured from a car on the freeway, yielding some interesting results[2].

The dominant feature of these distributions, obtained repeatedly over a two-day period, was a tri-modal distribution with a middle mode, centered mass-wise about 0.9 μm diameter, distinctly separated from two other modes with mass-median diameters of 0.12 μm and 4.3 μm. Figure 1 shows one such distribution, shown as differential normalized mass concentration versus aerosol diameter. By treating each of the three as a separate mode, as indicated by the dashed portions of the curve, three distinct log-normal distributions can be discerned, as shown in Figure 2. From these the relevant aerosol characteristics are derived and shown in the table below.

Mode	dm (um)	σ_g	dg	$\bar{d}$	dm	da	A	C (g/m^3)
1	0.12	1.75	0.047	0.055	0.075	0.064	8.5	1.08×10^{-4}
2	0.94	1.40	0.67	0.71	0.79	0.75	23.4	5.25×10^{-5}
3	4.3	1.32	3.4	3.5	3.8	3.7	34.4	2.41×10^{-5}

dm: Mass median diameter, micrometer
σ_g: Geometric standard deviation
dg: Geometric mean diameter
$\bar{d}$: Count mean diameter
dm: Mass average diameter
da: Area average diameter

A: Shape parameter, $(2 \log^2 \sigma_g)^{-1}$
C: Mass concentration, g/m^3
α_o: Size parameter, $\pi dg/\lambda$
λ: Wavelength
k_e: Extinction coefficient, m^2
k_s: Scattering coefficient

Using the computation results of Foitzik, et al[3], as presented in the Handbook on Aerosols by Dennis[4], the extinction coefficients and the forward scattering (10 degrees) coefficients for the three modes have been calculated, for three wavelengths, and the results are shown below:

Mode	σ_g	$\bar{d}$	A	α_o	λ	k_e	k_s
1	1.75	0.055	8.5	0.33	450	~0	~0
				0.27	550	~0	~0
				0.23	650	~0	~0
2	1.40	0.71	23.4	4.67	450	2.3×10^{-4}	3.0×10^{-5}
				3.82	550	2.4×10^{-4}	2.4×10^{-5}
				3.23	650	2.4×10^{-4}	2.0×10^{-5}
3	1.32	3.5	34.4	23.8	450	1.4×10^{-5}	9.4×10^{-6}
				19.5	550	1.4×10^{-5}	7.0×10^{-6}
				16.5	650	1.4×10^{-5}	5.8×10^{-6}

It is seen that Mode 1 is largely below the Mie scattering regime. Mode 2 satisfies the conditions derived by Porch[1]. Since forward scattering can be seen to be a dominant mechanism, the imaginary part of the refractive index has little influence. There is a decrease in the extinction coefficient with decreasing wavelength; but the main influence in the "blue headlight" observation appears to be the enhanced forward scattering with decreasing wavelength.

REFERENCES

1. William M. Porch, David S. Ensor, Robert J. Charlson, and Jost Heintzenberg, Applied Optics, 12, pp. 34-36, Jan. 1973.

2. Raymond L. Chuan, "Real Time Measurement of Aerosol Mass Distribution By Size" Ninth Aerosol Technology Meeting, October 21-22, 1976, Battelle Columbus Laboratories.

3. I. Foitzik, G. Hebermehl, and D. Spankuch, Optik, 23, 272 (1965/66).

4. Richard Dennis (Ed), "Handbook on Aerosols", Technical Information Center, Office of Public Affairs, U.S.E.R.D.A., TID-26608 (NTIS), 1976.

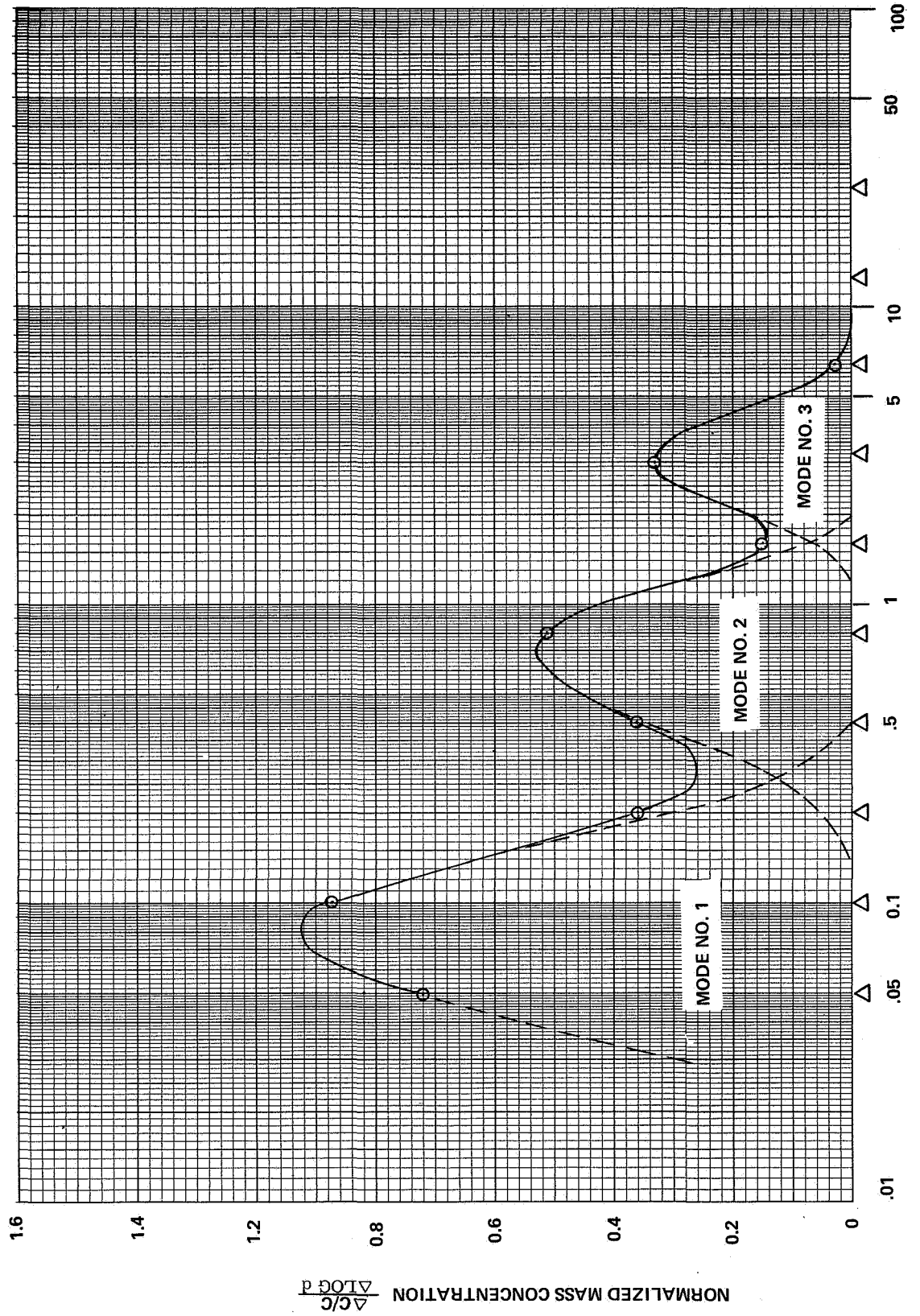

FIGURE 1. PARTICLE SIZE DISTRIBUTION

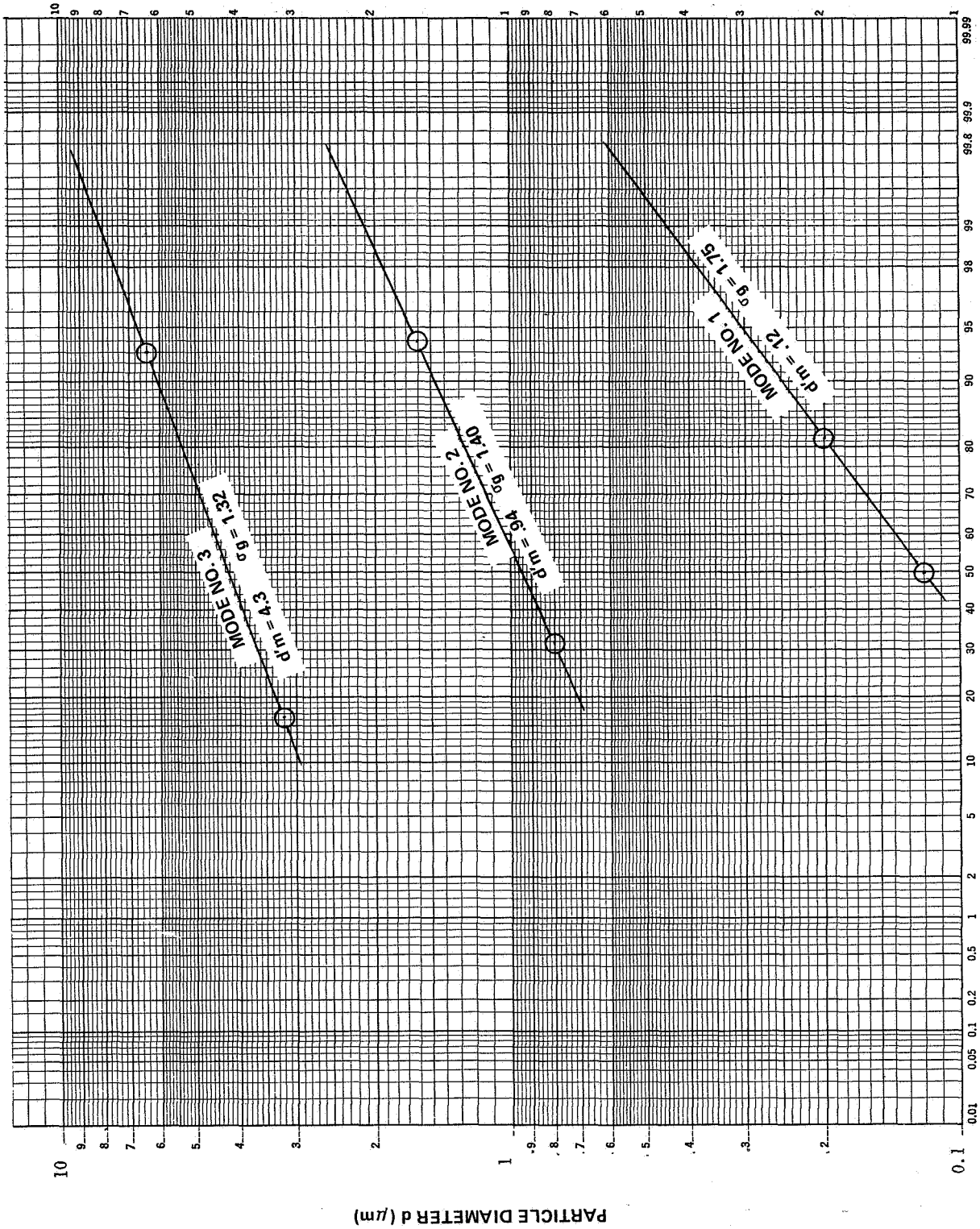

FIGURE 2. PARTICLE LOG-NORMAL DISTRIBUTION

PD2-1

Absorption Refractive Index of Aerosols in the Denver Pollution Cloud in the Interval .53 – .69 μ

J. J. DeLuisi
NOAA/ERL-ARL, Boulder, CO
J. E. Bonelli and C. E. Shelden
NCAR, Boulder, CO

OVERVIEW

Wideband spectral measurements of the global and direct solar flux at the surface were obtained at the Denver Trout Farm in conjunction with the EPA Denver Brown Cloud experiment on 20-21 November 1973. These measurements were analyzed by a simple variational technique to yield the increase in the rate of absorption and scattering by the Denver pollution cloud when the observed optical depth increased by approximately 0.06. The imaginary term of the complex refractive index of the aerosols is deduced from theoretical calculation data.

PROCEDURE

On 20 and 21 November 1973, observations of the direct and global solar flux at the earth's surface were obtained near the Denver Trout Farm. The direct beam is measured normal to the solar beam. The global flux is the sum of the skylight radiation and the direct beam incident on a horizontal receiver.

During the two-day period of measurement, the optical depth of the pollution layer increased by approximately 0.06 from the first to the second day and the solar flux reaching the earth's surface decreased by approximately 4.8% over the same time interval. The measured decrease in flux was ascribed to increased scattering and absorption by aerosols and gases in the polluted boundary layer.

The solar global flux impinging on a flat-plate receiver at the earth's surface is given by P where

$$P(\mu_0, m, \tau, r) = D(\mu_0, \tau) + S(\mu_0, m, \tau, r) \qquad (1)$$

where D is the direct radiation given by the expression

$$D(\mu_0, \tau) = \mu_0 F_0 e^{-\tau/\mu_0}, \qquad (2)$$

and where

μ_0 = cosine of the solar zenith angle; F_0 = the incident solar flux

m = complex refractive index of aerosols; r = surface reflectivity, and

τ = total optical depth of the atmospheric medium.

The S term in Eq (1) stands for the flux of the diffusely transmitted radiation which in our approximation is radiation scattered once downward after having been scattered from the direct beam, and back-scattered once downward after having been reflected by the earth's surface. Therefore, S depends on (1) surface reflectivity, (2) scattering and absorption optical depth of aerosols and gases, (3) solar zenith angle, and (4) the solar flux F_0 incident at the top of the optical medium. Surface reflectivity is important when there is substantial snow cover as in this work ($r \cong .5$)

The S term can be separated into S_f and S_r which are the forward scattered flux removed from the direct beam and the downward back-scattered flux (downwelling) arising from the flux reflected once by the surface, respectively.

If we take the derivative of Eq (1) with respect to τ_d, the optical depth of aerosols we have

$$\frac{\partial P}{\partial \tau_d} = \frac{\partial D}{\partial \tau_d} + \frac{\partial S_f}{\partial \tau_d} + \frac{\partial S_r}{\partial \tau_d} . \qquad (3)$$

We can express Eq (1) by an approximation having the form

$$P = \mu_0 F_0 e^{-\tau / \mu_0} + aK\mu_0 F_0 (1-e^{-\tau / \mu_0}) + r(1-a) K\mu_0 F_0 (1-e^{-\tau / \mu_0}) \qquad (4)$$

where a=0.82 (at a wavelength of 0.525 μ) is the fraction of power scattered downward and K, the unknown variable, is the fraction of power removed from the incident flux that is available for scattering. The term a is quite complicated for aerosol scattering, but it can be estimated in a formal way using Mie theory and a known aerosol size distribution.

Differentiating Eq (4) according to Eq (3), and solving for K we have

$$K = \frac{1}{a+(1-a)r} \left\{ 1 - \frac{\Delta P}{\Delta D} \right\} \qquad (5)$$

where $-\Delta D = F_0 e^{-\tau / \mu_0} \Delta\tau_d$ (for a horizontal receiver)

which is the change in power removed from the direct beam in finite difference form.

MEASUREMENTS

Radiant flux measurements were made with commercially available radiometers. The total flux was measured using three Eppley Model 2 pyranometers, one in each spectral band of interest. The direct normal flux was measured with an Eppley model 15 pyrheliometer equipped with a three position rotary filter holder. WG7,OG1 and RG8 Schott filters provided the spectral resolution. The pyranometers and pyrheliometer were not intercalibrated, nor do they need to be.

Figure 1 provides a summary of the analysis, following the procedure described above. It is evident from the figure that comparatively strong absorption is taking place in the OG1 and RG8 bands.

RESULTS

The work by Herman et al. (1975) provided us with a means to estimate a refractive index for the particulate materials in the brown cloud. We assumed all absorption in the OG1-RG8 band is due to particles having a size distribution approximated by $dN/d\log r \approx bl^{-2}$, *where N is particle number, l is particle diameter, and b is a constant. Assuming also that the real term of the complex refractive index is 1.5 (Bhardwaja et al., 1974), then the imaginary term can be deduced from functions similar to those of Herman et al., (1975): percent absorption incident solar power versus absorption refractive index for a specified solar zenith angle, surface albedo and aerosol optical depth. Following this procedure, we arrived at an approximate value of -0.03 for the imaginary term. This value is rather large, but is consistent with the strong absorption occurring within the cloud. Simultaneous radiation absorption by molecules will fictitiously increase the magnitude of the absorption refractive index. We believe it is impractical to estimate a figure of uncertainty on the value (in view of the uncertainties connected with the data), other than to state that it may be quite large, and that our estimate is probably an upper limit.*

Our refractive index can be compared with the results of other investigations of an urban atmosphere. Eiden (1966) deduced a range of -0.01, -0.1 for Mainz from polarization data, and Lin et al., (1973) deduced values ranging from -0.028 to -0.05 for New York City air, using the opal glass technique.

REFERENCES

Bhardwaja, P. S., J. Herbert, and R. J. Charlson: Refractive index of atmospheric particulate matter: an in-situ method for determination. Appl. Optics, 13, 731, (1974)

Eiden, R: The elliptical polarization of light scattered by a volume of atmospheric air. Appl. Optics, 5, 509, (1966)

Herman, B. M., S. R. Browning, and J. J. DeLuisi: Determination of the effective imaginary term of the complex refractive index of atmospheric dust: the diffuse-direct radiation technique. J. Atmos. Sci., 32, 918, (1975)

Lin, C. I., M. Baker, and R. J. Charlson: Absorption coefficient of atmospheric aerosol: A method for measurement. Appl. Optics, 12, 1356, (1973)

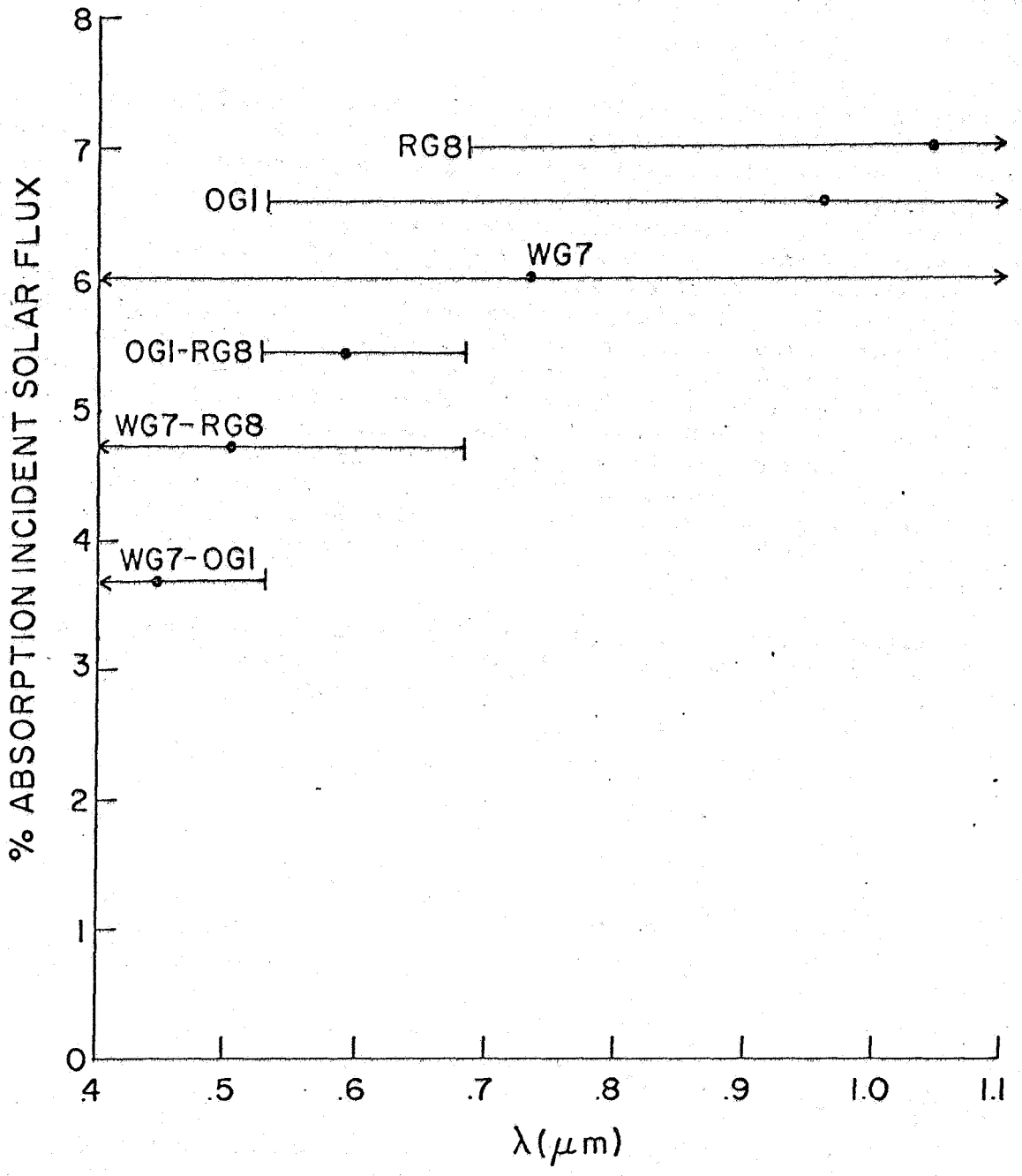
% ABSORPTION INCIDENT SOLAR FLUX
λ(μm)
RG8
OGI
WG7
OGI-RG8
WG7-RG8
WG7-OGI
0
1
2
3
4
5
6
7
8
.4
.5
.6
.7
.8
.9
1.0
1.1

Fig. 1

A TWO-DIMENSIONAL STRATOSPHERIC MODEL OF THE DISPERSION OF AEROSOLS FROM THE FUEGO VOLCANIC ERUPTION

Ellis E. Remsberg, NASA Langley Research Center, Hampton, Virginia 23665
Carolyn F. Jones, Old Dominion University, Norfolk, Virginia 23508
Jae H. Park, College of William and Mary, Williamsburg, Virginia 23185*

Observational data of the pre- and post-volcanic aerosols have been used in conjunction with predictions of a 2-D circulation model to gain better understanding of the transport, chemical, and sedimentation processes for the stratospheric layer. This paper specifically concerns the Fuego eruptions in Guatemala (15°N) in October 1974. A lidar measure of aerosol mixing ratio used for observational data in this paper is the scattering ratio, $R_s = 1 + f_a/f_m$, where f_a and f_m are the aerosol and molecular backscattering functions, respectively. The f values are products of the species cross section and number density. Figure 1 shows two R_s profiles obtained by lidar at Hampton, Virginia. The plot for January 2, 1975, represents an enhanced aerosol layer due to Fuego volcanic activity. The February 19, 1976, profile resembles a near-background aerosol level and shows the depletion of the January 2 layer over 13 months (ref. 1). Any R_s value greater than one represents backscattering from aerosols. If the aerosol cross section is constant with height, the scattering ratio profile is a direct measure of aerosol number density.

The aerosol distribution is predicted by the model in the form of $\chi(t) = \chi(t_o) + (d\chi/dt)\Delta t$ where the rate of change of aerosol mixing ratio is defined by $d\chi/dt = (\partial\chi/\partial t)_{ch} + (\partial\chi/\partial t)_{gr} + (\partial\chi/\partial t)_{tr} + (\partial\chi/\partial t)_{sed}$. χ is the aerosol mixing ratio, $(\partial\chi/\partial t)_{ch}$ is the chemical term, $(\partial\chi/\partial t)_{gr}$ is the aerosol growth term, $(\partial\chi/\partial t)_{tr}$ is the transport term, and $(\partial\chi/\partial t)_{sed}$ is the sedimentation term. The numerical integration is performed from initial time, t_o, to final time, t, at intervals of Δt. Since the gas-to-aerosol chemistry is not well understood, the modeling attempt in this paper does not consider the term $(\partial\chi/\partial t)_{ch}$. Also, because the processes of aerosol growth are only understood qualitatively (ref. 2), they have not been incorporated into the model calculations at this time.

The dynamical model developed by Louis (ref. 3) includes advection by the mean meridional circulation and diffusion by large-scale eddies. The model extends from 0 to 50 km in altitude with a grid spacing of 1 km, and from 90°N to 90°S with a grid spacing of 5°. For simulations presented in this paper, the circulation has been specified by monthly mean winds and eddy diffusion parameters derived from Louis' Model II. Mean winds for the winter season are shown in figure 2. Louis' model has successfully approximated the distribution of radioactive debris in the stratosphere. In particular, the analysis of a volcanic event

*Jae Park is supported by NSF DES75-14228 for this work.

represents dispersion from a point source, siimilar to that for radioactive bomb debris.

Hunten (ref. 4) has discussed the importance of aerosol sedimentation rates for determining the residence times of volcanic aerosol layers. Aerosol fall speeds for various aerosol sizes tabulated by Kasten (ref. 5) for particle densities of 1.5 g/cm^3 have been applied to an initial aerosol size distribution. An estimate of the Fuego aerosol size distribution has been adopted from the 1963 measurements by Mossop (ref. 6) which were obtained 1 month after the eruption of Mount Agung. The total size distribution has been divided into four size ranges with mean radii of 0.16 μm, 0.32 μm, 0.53 μm, and 0.93 μm. Distributions of mass mixing ratios of four different sizes are then calculated as functions of altitude and time.

Initially, it is assumed that any substantial deviations between the model results and the observed aerosol profiles can be accounted for within the uncertainties in the aerosol sedimentation, growth rates, and chemistry.

High resolution infrared satellite photographs (released by the National Oceanic and Atmospheric Administration in Rockville, Maryland) were employed to estimate the initial location (shown as a dot in fig. 2), size, and direction of the dust clouds for several days after the eruptions of October 14 and 17, 1974. The model is started on October 19 at 1200Z to allow for some spread of the cloud. Data taken by lidar at Hawaii (ref. 7) on October 29 were applied to verify the initial vertical profile of the dust layer. The vertical width of the layer at half maximum as computed by the model for October 29 at 20°N was compared with the observations (half-width of 0.8 km) at Mauna Loa Observation in Hawaii. The shapes of the model profiles at all latitudes where aerosol had been transported in that 10-day period were adjusted to agree with the Hawaii observations. These adjusted profiles then represent the initial conditions for the aerosol source. Amounts of injected material were determined from estimates by Cadle, et al. (ref. 8). A constant mass mixing ratio of 2×10^{-10} was assumed for the model at a lower boundary of 10 km. Dustsonde data from Wyoming (ref. 9) support the assumption that the aerosol mixing ratio in the upper troposphere remains almost constant with time after the eruption.

Figure 3 displays the integrated aerosol mass density between 16 and 21 km as a function of time after the eruption. The solid line represents the lidar data from Hampton, Virginia (37°N). The lidar data were obtained by summations over 1 km increments of $(\bar{R}_s(Z) - 1)\, N_m(Z)$ where $\bar{R}_s(Z)$ is the average scattering ratio and $N_m(Z)$ is the molecular number density. The quantity on the ordinate is then equivalent to $(\sigma_a/\sigma_m)\, N_a(Z)$ where σ_a and σ_m are aerosol and molecular cross sections, respectively, and $N_a(Z)$ is the aerosol number density which is directly proportional to aerosol mass density. No attempt has been made to actually compute mass densities from the lidar data. The model results in figure 3 are an average for 35°N and 40°N latitude. The model quantity is a little

different from observed quantities because it does not contain the additional effects of a time-varying size distribution as does the scattering ratio lidar measurements which are more sensitive to larger size particles. The circles in the figure are for a log-normal background type aerosol size distribution (ref. 10) where the mean radius is 0.0725 μm. The triangles are for a volcanic aerosol size distribution taken from Mossop (ref. 6). The model results in figure 3 clearly show that vertical aerosol profiles and aerosol residence times are sensitive to the sedimentation term, as well as the transport term.

The peak magnitudes of the lidar and model data have been arbitrarily adjusted to afford a better comparison of the time rate of change of the aerosol column load. The time of the occurrence of the maximum aerosol load has been simulated very well by the model, indicating that the meridional transport for the first few months is reasonable. The 1/e decay time for the integrated aerosol column density from lidar measurements (16-21 km) after February 1975 is about 10 months. It is important to note that longitudinal movements of aerosol clouds, displayed in the observational data as periodic peaks, are not simulated in the present zonally averaged model.

Figure 4 shows the initial size distribution adopted from Mossop for the Agung eruption for 20 km and 15°N to 35°S latitude and then compares subsequent measured size distributions with those determined from the model by including sedimentation processes. In general, the comparison is reasonable. The initial size distribution employed in this model may, however, contain too many large particles. The sedimentation rates may be too rapid, which would affect the results shown in figure 3 as well. Comparative vertical profiles of mass mixing ratios will not be presented in this paper.

The initial study into the dispersion of volcanic particles has shown that transport alone does not account for the spread to other latitudes and altitudes. To obtain more accurate sedimentation rates, it will be necessary to have more post-volcanic particle size distribution data. The aerosol chemistry may be of importance and should be included in further studies. Quantitative knowledge of aerosol growth by gas condensation must also be considered.

REFERENCES

1. Remsberg, E. E.; and Northam, G. B.: A Comparison of Dustsonde and Lidar Measurements of Stratospheric Aerosols. Proceedings of the Fourth Conference on the Climatic Impact Assessment Program (CIAP), Department of Transportation, 1976, pp. 509-518.

2. Turco, R. P.; Hamill, P.; Toon, O. B.; and Whitten, R. C.: A Model of the Stratospheric Sulfate Aerosol. NASA CP-2004, Dec. 1976.

3. Louis, J. F.: A Two-Dimensional Transport Model of the Atmosphere. Ph.D. Thesis, University of Colorado, 1974.

4. Hunten, D.: Residence Times of Aerosols and Gases in the Stratosphere. Geophys. Res. Let., Vol. 2, 1975, pp. 26-28.

5. Kasten, F.: Falling Speed of Aerosol Particles. J. Appl. Meteor., Vol. 7, 1968, pp. 944-947.

6. Mossop, S. C.: Volcanic Dust Collected at an Altitude of 20 km. Nature, Vol. 203, 1964, pp. 824-827.

7. Fegley, R. W.; and Ellis, H. T.: Lidar Observations of a Stratospheric Dust Cloud Layer in the Tropics. Geophys. Res. Let., Vol. 2, 1975, pp. 139-141.

8. Cadle, R. D.; Kiang, C. S.; and Louis, J. F.: The Global-Scale Dispersion of the Eruption Clouds From Major Volcanic Eruptions. J. Geophys. Res. , Vol. 81, 1976, pp. 3125-3132.

9. Hofmann, D. J.; and Rosen, J. M.: Balloon Observations of the Time Development of the Stratospheric Aerosol Event of 1974-75. Report AP-36, Dept. of Phys. and Astron., University of Wyoming, 1976.

10. Pinnick, R. G.; Rosen, J. M.; and Hofmann, D. J.: Stratospheric Aerosol Measurements III: Optical Model Calculations. J. Atmos. Sci., Vol. 33, 1976, pp. 304-314.

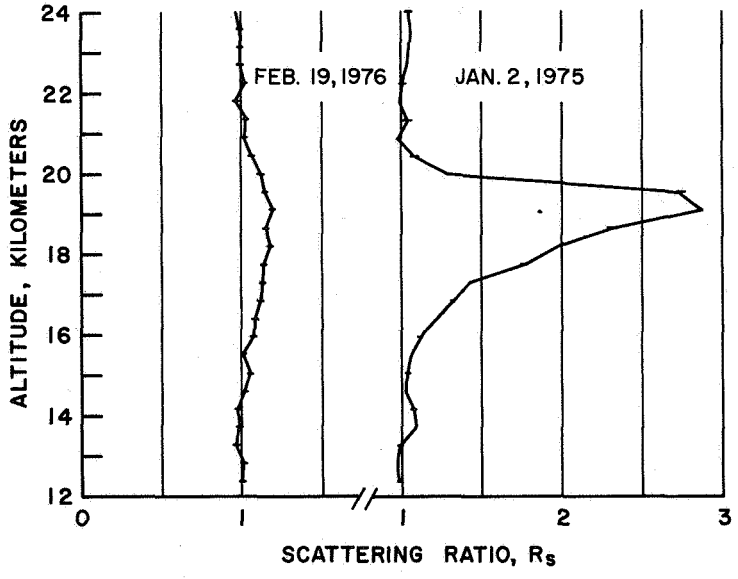

Figure 1

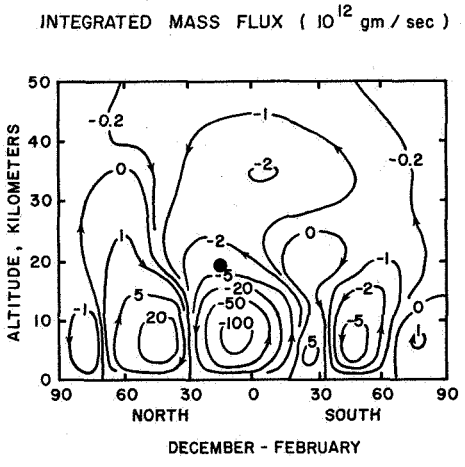

Figure 2

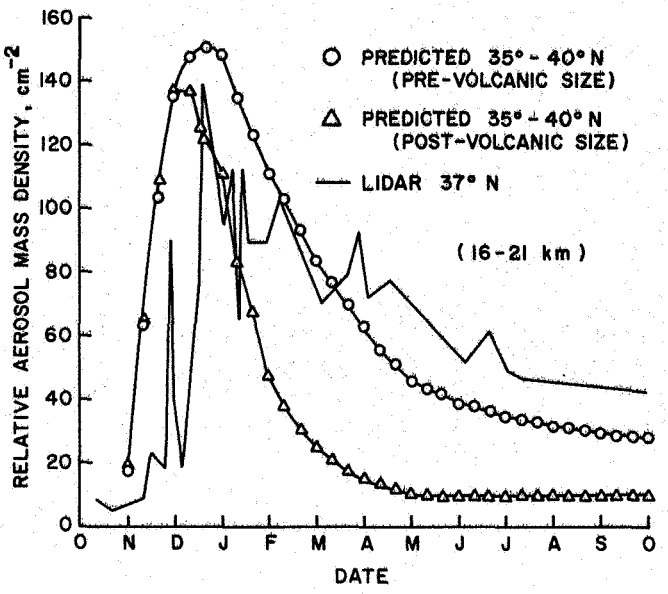

Figure 3

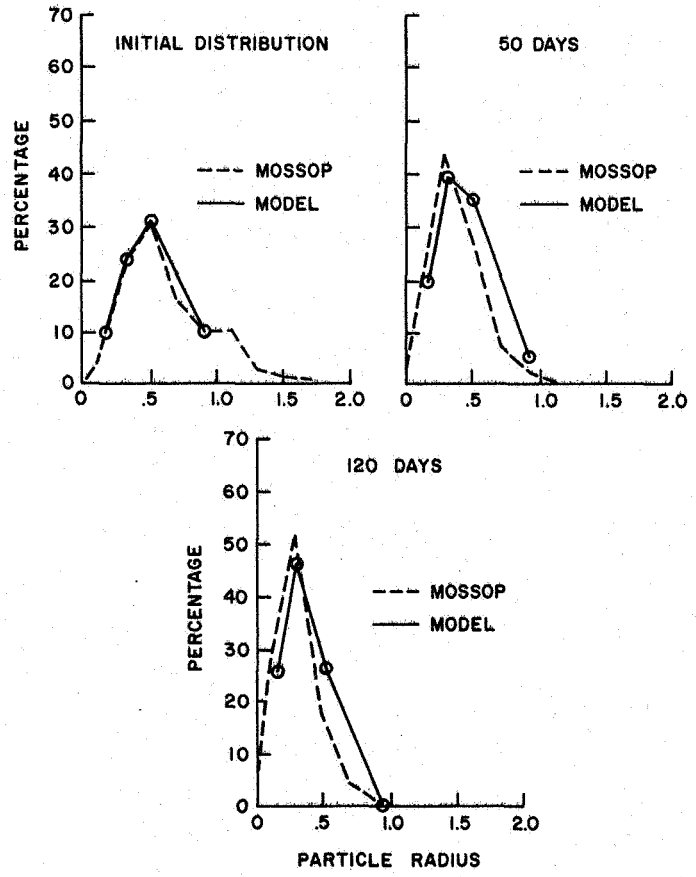

Figure 4

ON THE VARIATION OF THE AEROSOL VOLUME TO LIGHT SCATTERING COEFFICIENT

by

George M. Sverdrup* and Kenneth T. Whitby

Department of Mechanical Engineering
University of Minnesota

*Present Address: Battelle, Columbus Laboratories
Columbus, Ohio

A number of investigations have been conducted relating aerosol mass concentration to the aerosol light scattering coefficient b_{sp} (m^{-1}). These studies, reviewed by Charlson (1969), suggested that the ratio of aerosol mass or volume to b_{sp} was approximately a constant, and that this relationship could be used on a practical basis to infer the aerosol mass concentration from b_{sp}.

The present work examines the variation of the ratio, K_p, of submicron aerosol volume, V3 - ($\mu m^3/cm^3$), to b_{sp}. The experimental data were acquired in the California Aerosol Characterization Experiment (ACHEX) during 1972 and 1973. V3 - was determined using the Minnesota Aerosol Analyzing System (Whitby, et al., 1975). An integrating nephelometer was used to determine b_{sp}.

The variation of K_p as a function of the total aerosol number concentration, CNC ($No./cm^3$), determined with a condensation nuclei counter is shown in Figures 1 and 2. K_p ranges from 5 to 80. Near combustion sources large quantities of particles with sizes below the light scattering range were added to the distribution increasing V3 - significantly but not affecting b_{sp} appreciably. Thus as CNC rose, K_p became greater.

The data fall into groups which can be identified with general location. Six categories are shown in Figures 1 and 2. Aged aerosols have values of K_p in the range 6 to 20 $\mu m^3/cm^3 \times m \times 10^{-4}$. Fresher aerosols, e.g., categories D and F, have values of K_p in the range 20 to 80. The two nonurban categories have values of CNC less than 20,000 cm^{-3}. Urban areas not influenced by strong combustion sources have concentrations between 20,000 and 250,000 cm^{-3}.

The variation of K_p was examined theoretically by modeling the aerosol size distribution with a composite distribution made up of 3 log-normal functions. These components correspond to the nuclei, accumulation and coarse particle size distribution modes (Whitby, 1975). The variation of K_p was studied by computing the value of K_p from the model distribution using Mie theory to predict b_{sp}. A two-dimensional nephelometer geometry was used. The light scattering efficiency was computed by integration over the nominal spectral response of the nephelometer using a refractive index of 1.50-0.02 i. The initial model distribution was the fit to the grand average measured distribution from Goldstone, CA. The concentration of the nuclei mode was then varied in order to simulate different aerosol sources.

The resulting variation of K_p is shown as the dashed curve in Figure 1. The conclusions to be drawn from this work are

(1) The large variations in K_p (i.e., 5 to 80) preclude its use as a good indicator of submicron aerosol volume or mass concentration.

(2) Using the particle number concentration and K_p, aerosols can be classified according to general location.

(3) Variations in aerosol size distributions are enough to account for the observed variation of K_p.

References

1. Charlson, R.J. (1969), "Atmospheric visibility related to aerosol mass concentration: A review", Environ. Sci. Technol., 3:913-918.

2. Whitby, K.T., Clark, W.E., Marple, V.A., Sverdrup, G.M., Sem, G.J., Willeke, K., Liu, B.Y.H., and Pui, D.Y.H. (1975), "Characterization of California aerosols - I. Size distributions of freeway aerosol", Atmos. Environ., 9:463-482.

3. Whitby, K.T. (1975), "Modeling of atmospheric aerosol particle size distributions", Progress Report EPA Grant R 800971, University of Minnesota.

Acknowledgment

The measurements were made under Contract No. 358 from the California Air Resources Board.

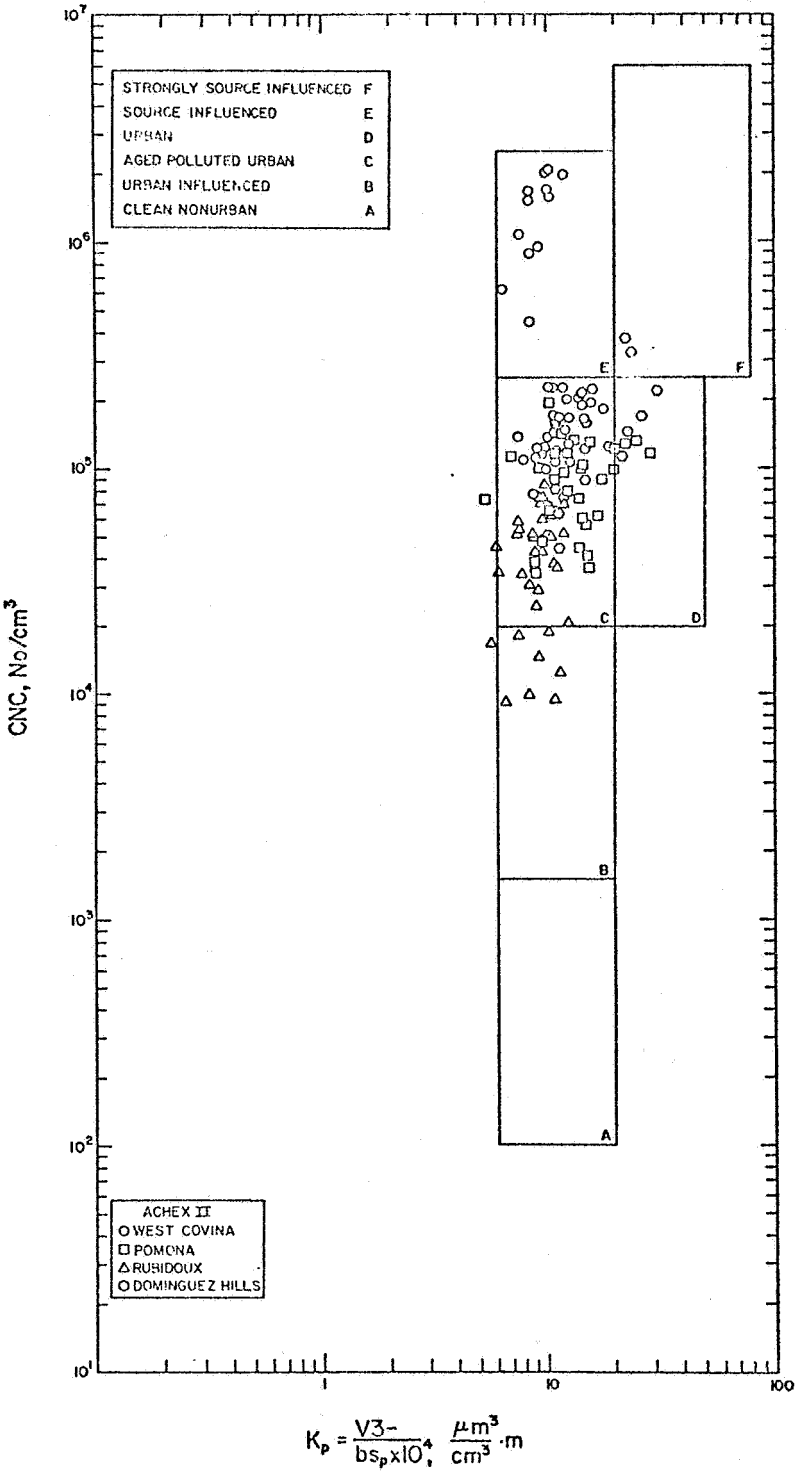

Figure 2 Variation of the aerosol submicron volume to aerosol light scattering coefficient with the total aerosol number concentration from ACHEX II.

Spectrophone In Situ Measurements of the Absorption of Visible Light by Aerosols

R. W. Terhune and J. E. Anderson
Research Staff, Ford Motor Company, Dearborn, Michigan 48121

In extinction measurements of visible light by atmospheric aerosols, the effects of absorption are usually masked by scattering. Separate absorption measurements would aid greatly in interpreting extinction data and characterizing aerosols. It would also allow one to evaluate the contribution of visible sunlight absorption by atmospheric aerosols to the radiation balance of the earth.[1,2] Aerosol absorption properties are usually deduced from measurements of the optical properties of collected samples and measured particle size distributions.[3] In a paper at this meeting, Patterson, Gillette and Stockton[4] report on their recent measurements of the complex index of refraction of aerosols from 300 to 700 nm. Also, Bruce and Pinnick[5] report at this meeting some infrared spectrophone in situ aerosol absorption measurements.

We report here in situ measurements of the absorption by atmospheric aerosols in the visible near 514.5 nm. We used a 1/2 watt 514.5 nm argon laser beam chopped at 4000 Hz to drive a spectrophone. Light absorption led to localized heating. The associated gas expansion in the cavity generated a sound wave which was detected with a microphone.

In the case of absorption of light by aerosols, sound generation is limited by the rate at which heat is transferred to the gas. The thermal time constant of the particles is proportional to the square of their diameter.[6] At 4000 Hz, heat transfer is efficient for spherical particles less than about 3 microns in diameter. For atmospheric measurements, it would be desirable to detect the absorption in particles up to about 20 microns by operating at 90 Hz or less. One can use this particle-size dependence of the time constant to determine the absorption contributions from different particles.

In order to obtain enhanced sensitivity, a resonant acoustic cavity was used in the spectrophone.[7,8,9] A cylindrical brass cavity, 5-cm in diameter and 15-cm long, was used in its lowest order circumferential mode which had a Q of 250. The laser beam was passed through the cavity near one wall, entering and leaving through 8-mm diameter holes in the end walls. A 1-inch B&K condenser microphone with a sensitivity of 42 mV/Pa was mounted flush with the cavity wall on the opposite side. Synchronous detection was used. An acoustic signal of about 1.1 Pascals rms per m^{-1} absorption per watt of laser power was obtained. An rms noise level of about 0.01 μV $sec^{-1/2}$ was observed after synchronous detection. Acoustic isolation was achieved by placing the cavity inside three sound insulating boxes, one inside the other. Measurements were made with gas flowing at a rate of 2 ℓ/min. The system was calibrated by observing the absorption of 30 ppm NO_2 in air which was measured to be around 180×10^{-4} m^{-1}. The above numbers indicate a system detection limit (S/N ratio = 1) of 2×10^{-7} m^{-1} in one second with a single pass of a one-watt laser.[7] The acoustic circuit including the detection system design has not been optimized.

Measurements with an integrating nephelometer indicated an extinction of around 2.5 times Rayleigh scattering in the room air. The absorption measurements in the room air shown in the figure indicate an absorption of 10^{-5} m^{-1}, probably due to aerosols with diameters less than 3 microns. The residual absorption after filtering is about what one would expect from 3 ppb of NO_2.

A quick series of experiments were carried out with NaCl and $NiCl_2$ aerosols made by aspirating water solutions. Other experiments used cigarette smoke. The aerosols were blown through the cavity. Scattering measurements were made with an integrating nephelometer sampling the exiting stream of aerosols. The results are summarized in the table.

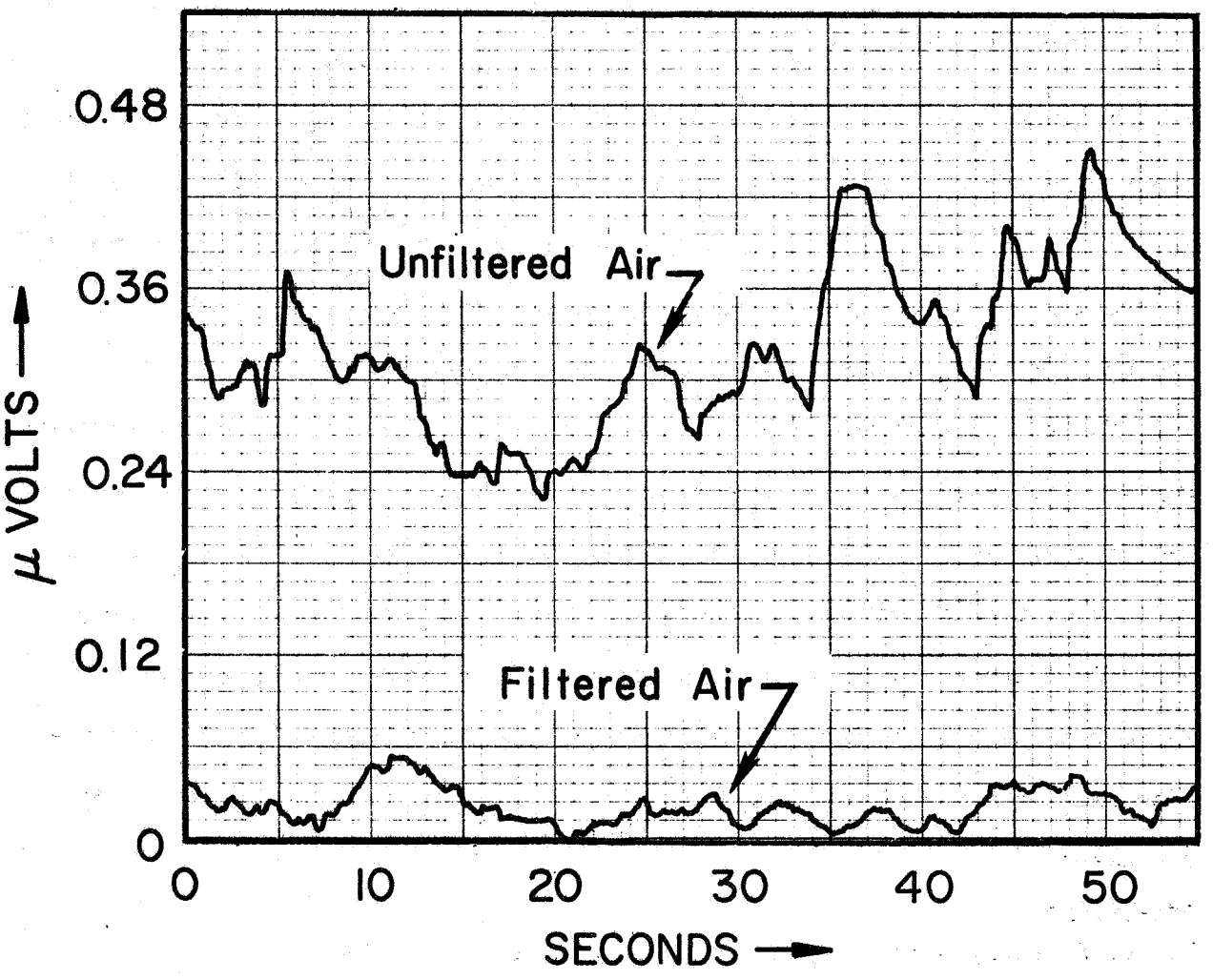

Recorder traces showing the observed synchronously detected spectrophone signal with and without aerosols. A millipore filter with a 10-nm pore size was used. The large fluctuations in the signals with ulfiltered air can probably be associated with fluctuations in the number of particles illuminated by the 1-mm diameter laser beam in the spectrophone. 0.12 μ volts corresponds to an extinction coefficient due to absorption of 0.5×10^{-5} m^{-2}. The extinction coefficient due to Raleigh scattering in air at this wavelength is about 10^{-5} m^{-1}.

Aerosol Extinction Coefficients Relative to Rayleigh Scattering

	Scattering	Absorption	Ratio
NaCl	50	<0.2	<0.004
$NiCl_2$	50	1.5	0.03
Cigarette Smoke - through	250	200	0.8
Cigarette Smoke - off tip	15	100	7

The NaCl experiments demonstrate the insensitivity of the spectrophone to scattering per se. Here only transparent aerosols are expected. Our analysis indicates that only about 10^{-4} of the scattered light would be effective in generating acoustic signals following absorption in the cavity walls. In the case of $NiCl_2$, a small amount of absorption was found as expected.

For the aerosol drawn through the cigarette, the absorption and scattering were observed to be about equal, which one would expect for an aerosol of medium to large particles of optically lossy material. For the aerosol off the tip of the cigarette, the absorption is much larger than the scattering which is characteristic of small particles of optically lossy materials. These results are generally consistent with the differences in the particle size distributions observed by Whitby el al. for cigarette aerosols in the two cases.[10]

References

1. R. H. Reck, Science, Vol. 186, 15 July 1974, p. 1034.
2. S. I. Rasool and S. H. Schnieder, Science, Vol. 173, 9 July 1971, p. 139.
3. C-I Lin, M. Baker and R. J. Charlson, Applied Optics, Vol. 12, No. 6, June 1973, p. 1356.
4. E. M. Patterson, D. A. Gillette and B. H. Stockton, to be published.
5. C. W. Bruce and R. G. Pinnick, to be published.
6. C. H. Chan, Appl. Phys. Lett., Vol. 26, No. 11, 1 June 1975, p. 628.
7. C. F. Dewey Jr., R. D. Kamm and C. E. Hackett, Appl. Phyl Lett. Vol. 23, No. 11, December, 1973, p 633.
8. Paul D. Goldan and Kenya Goto, J. of Appl. Phys., Vol. 45, No. 11 Oct. 1974, p. 4350.
9. E. Max and L. G. Rosengren, Opt. Comm., Vol. 11, No. 4, Aug. 1974, p. 422.
10. K. T. Whitby et al., U. of Minn., Particle Lab. Publ. No. 137, July 1969.

THE KRAKATOA VOLCANIC TURBIDITY - A REASSESSMENT

Frederic E. Volz
Atmospheric Optics Branch, Air Force Geophysics Laboratory
L. G. Hanscom AFB, Bedford, MA 01731

The explosions of Krakatoa volcano in August 1883 (Symons 1888) are considered to have been the strongest volcanic event in the last 150 years. Tremendous amounts of ash reduced the solar radiation for some years. The general effect of volcanic dust on climate is still unsettled. Nevertheless, using dust data since the Krakatoa eruption, Oliver (1976) could obtain close agreement with observed northern hemispheric surface temperature variations.

A great number of worldwide reports of visual observations of abnormal twilight and skylight phenomena due to the Krakatoa dust has been summarized and discussed (Symons 1888, and others). There have been recent attempts to quantitatively discuss some aspect of the dust event (Deirmendjian 1973, Dyer 1974) but measurements hitherto not considered make possible a more detailed and balanced account. Also, more recent data allow to develop more generally the fate of stratospheric dust of a tropical source.

In the period of the Krakatoa event (since 1875) solar radiation was measured only at Montpellier (42N), at the French Mediterranean. Monthly averages of the noontime intensities presented by Kimball (1918) and used again by Dyer (1974) show the greatest turbidity about 2 years after the explosion. Having been intrigued by the long delay and possibility of large seasonal variations, I examined the original data and came to the following conclusions: (1) Turbidity at this sea level locality varied greatly so that averages of months with few measurements are very questionable. (2) As shown in Fig. 1a, volcanic aerosol optical thickness τ_A was about 0.15 during 1884 and 0.10 in 1886 when other sky phenomena were said to have faded out (see Fig. 1c and d), and seem to have been recognizable as late as 1888 and 1889 (eruptions by other volcanoes in 1886 and 1888 seem to have been minor). Comparing radiation maxima only, volcanic turbidity appears to have been about 30% larger (Fig. 1b).

Some measurements of the position of neutral points of sky polarization in Germany (Busch 1889) between late 1886 and late 1888 (Figs. 1d and 2) confirm that volcanic turbidity ($\tau_A \approx 0.02$) still was present by early 1888. Also, the moon was still very dark in eclipses of 1888 and 1889.

Reports from the inner tropics of heavy sky haze, dim and colored suns even at noontime, and the Bishop ring have, as well known, shown that the fresh Krakatoa dust cloud circled the earth twice from east to west in 2 weeks

time. The few reports of the sun disappearing before setting in striated haze of strange colors lead, based on our corresponding observations in heavy summer haze, to estimates of $\tau_A \approx 0.45$, 0.60 and 1.6 (Deirmendjian 1973 used 0.65). However, these seem to have been extreme cases before the dust got more evenly distributed. Indeed, 2 months after the eruption there weren't any more relevant reports from the tropics, although Bishop rings and purple lights lasted at least until 1886.

We, therefore, evaluated as in our Katmai study for higher latitude sources (Volz, 1975) nuclear debris data from sources in the near-tropical stratosphere. As Fig. 3 shows the steady state vertical debris load increases toward the poles by more than a factor 2. This apparent paradox follows from the fact that the peak mixing ratio in the relatively thin debris layer, which slants from about 24 km in the tropics to 14 km in the Arctic, decreases along this profile less than the air density. Indeed, the evaluation of solar data of the Agung period by Dyer and Hicks (1965) suggests constant average turbidity between 18N and 81N, and shows notably higher turbidity at the South Pole than at the same time at 30-40S (the high turbidity derived for 0-10S is, at least with regard to the Congo data, very questionable as are the northern hemisphere minima).

The decrease of midlatitude ($\sim$45N) turbidity from great tropical volcanic eruptions is shown in Fig. 4, superimposed by the year of eruption, and taking data by Dyer (1974) into account. About 1.5 years after the eruption, Krakatoa turbidity is higher by a factor 5 than Agung turbidity (crude global average), and then abates with a residence time of about 1.5 years. That, according to lidar data, the small Fuego turbidity vanished much faster is attributable to its confinement to altitudes below 19-20 km even in the tropics. Tropical twilight observations gave altitudes of 25-35 km for the Krakatoa cloud, and indeed easterly winds of 30m/sec as derived from the drift of the fresh cloud do not seem to normally exist below about 24 km (Belmont and Dartt, 1970).

There are more problem areas of the optics of the Krakatoa dust, which briefly will be mentioned. Thus, the influence of heavy sky haze on twilight phenomena, notably the possibility to derive the layer altitude from visual observations when extinction becomes dominant, deserves attention. Very interesting is also the size distribution. While the radius derived from the globally reported Bishop ring is about 0.6μm, this size cannot - as Deirmendjian (1973) pointed out - have been very predominant because the sun was normal red, and not green, at setting except early in the tropics. Otherwise, this Bishop ring might be related to the difference of the Arago neutral points in Krakatoa and Katmai twilights (Fig. 2).

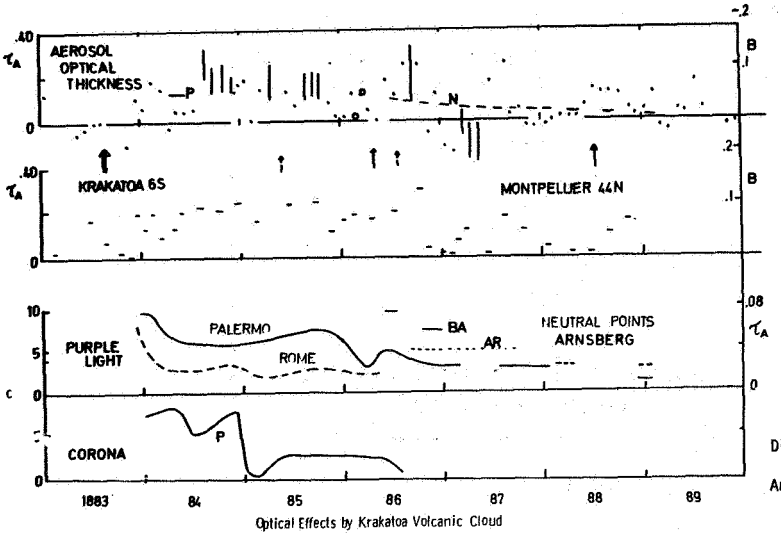

Optical Effects by Krakatoa Volcanic Cloud

Fig. 1

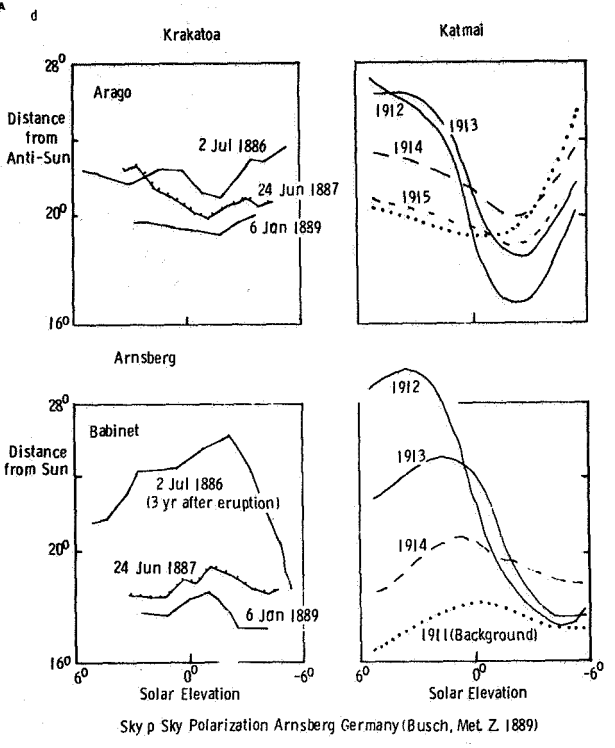

Sky p Sky Polarization Arnsberg Germany (Busch, Met. Z. 1889)

Fig. 2

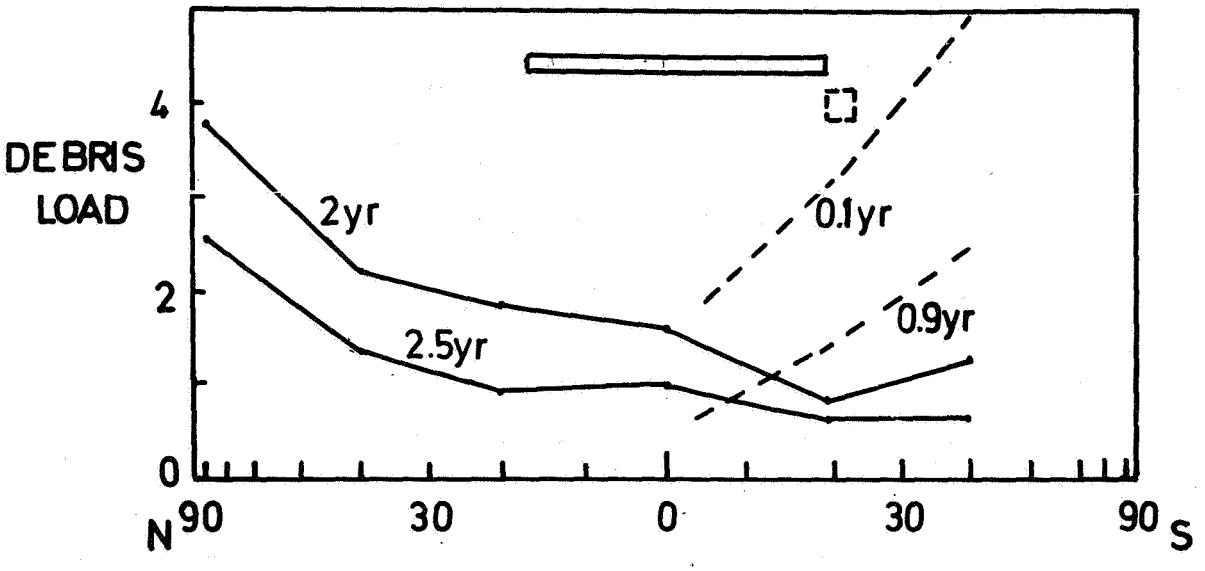

Fig. 3. Latitude distribution of nuclear debris vertical load (US tests 2N and 17 N. April and Nov. 1962) Numbers: year after event.

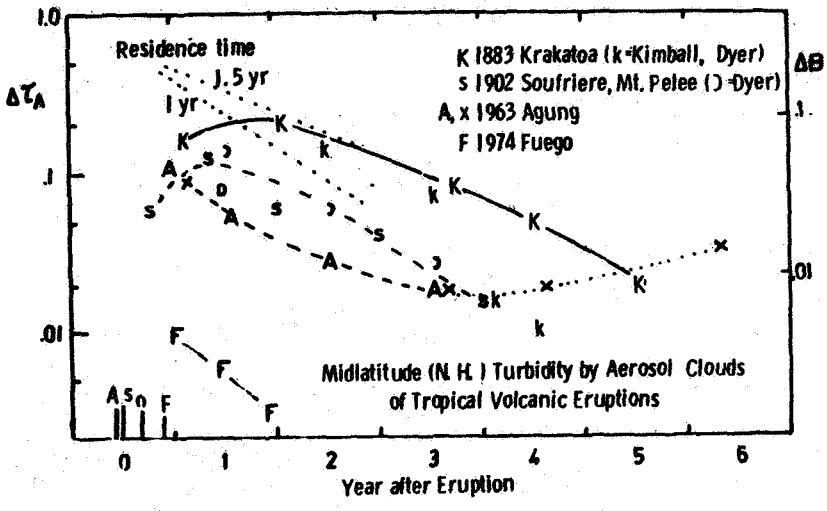

Fig. 4. Comparison of turbidity at about 45N from tropical-stratospheric volcanic dust source.
Global aerosol load, 0.3 years after eruption, for Krakatoa 34, Katmai 13, Agung 9, Fuego 1.5(mio tons).

References

Belmont, A.D., and D. G. Dartt, 1970: J. Geophys. Res. 75, 3130-3137.

Busch, F., 1889: Meteor. Zeits. hr. 6, 81-89.

Deirmendjian, D., 1973: Adv. in Geophysics, 16, 267-296.

Dyer, A. J., 1974, Quart. J. Roy. Met. Soc. 100, 563-571.

Dyer, A. J. and B. B. Hicks, 1965, Nature 208, 131-133.

Kimball, H. H., 1918: Monthly Wea. Rev. 46, 355-356.

Oliver, R. C., 1976: J. Appl. Meteor. 15, 933-950.

Ricco, A., 1887: Annali d. Meteorologica Italiana, 1885, 7, Parte I, 250-462 (Roma).

Symons, G. J. (Ed.), 1888: The eruption of Krakatoa and subsequent phenomena, report of the Krakatoa committee, 497 pp., Truebner and Co., London.

Volz, F.E., 1975: J. Geophys. Res. 80, 2649-2652.

Multiple Scattering in the Sky Radiance

by Bary de, E. and Bullrich, K.
Institut für Meteorologie, Johannes Gutenberg-Universität,
6500 Mainz, Germany

Multiple scattering is defined as scattering of higher order plus reflected radiation from the surface within the solar wave length range.
Distinct ways of the solution of the equation of radiative transfer, containing the multiple scattering, make it possible to calculate the sky radiance and its degree of polarization at any points in the sky for any altitudes in the atmosphere. That means under distinct assumptions based on measurements of the optical properties of the particulate matter in the atmosphere, it is possible to compute the upward and downward radiative fluxes and their divergences. These divergences can be expressed as heating or cooling rates respectively at different heights in the atmosphere. These results are of great interest for the energy budget of the atmosphere.

The following pictures give examples a) of the amounts of the multiple scattering or the scattering of higher order respectively partly in the form relative to the amount of the primary scattering. b) They show the distribution of the portion of the multiple scattering in the sky. c) They demonstrate the influence of distinct optical properties of the particulate matter, namely the aerosol particles.

Fig. 1 Portions of the first, second and third scattering processes of sky light.

Fig. 2 Ratio of sky light including scattering of higher order over primary scattering only. T turbidity factor, m complex refractive index, wavelength λ = o.55 microns, surface albedo A = o, zenith-distance of the sun ϑ = 37°. The computated results are valid for sun_s vertical. Eschelbach, G. 1974.

Fig. 3 Percentage ratio of primary PS to total scattering TS, as a function of the scattering angle φ and the wavelength λ at the solar elevation of 24°. Surface albedo A = o.o. No aerosol absorption. The hatched surface marks the difference in the values of the sun's vertical and the solar almucantar. Turbidity factor T = 2. Bary de, E. and Eschelbach, G. 1974.

Fig. Three dimensional plot of surface of equal percentage of the ratio PS/TS. The orthogonal coordinate system has the angular distance from the sun (φ) as x-axis, the wavelength (λ) as y-axis and the turbidity factor (T) as z-axis. S.V. means sun's vertical . Surface albedo A = o.25, complex refractive index m = 1.5-o.oi Bary de, E. 1973.

References (only from Mainz)

1. Bary de, E. 1973: Beitr. Phys. Atm., 46, 1973
2. Bary de, E. and Eschelbach, G. 1974: Tellus XXVI, 6, 682
3. Danzer, K.H. and Bullrich, K. 1966/67: Optik, 24, 577
   Danzer, K.H. and Bullrich, K. 1968: Beitr. Phys. Atm. 41, 143
4. Eschelbach, G. 1971: J. Quant. Spect. Rad. Transfer, 11, 757
5. Eschelbach, G. 1973: Ann. Geophys. 29, 329
6. Heger, K. 1971: Beitr. Phys. Atm. 44,2o1

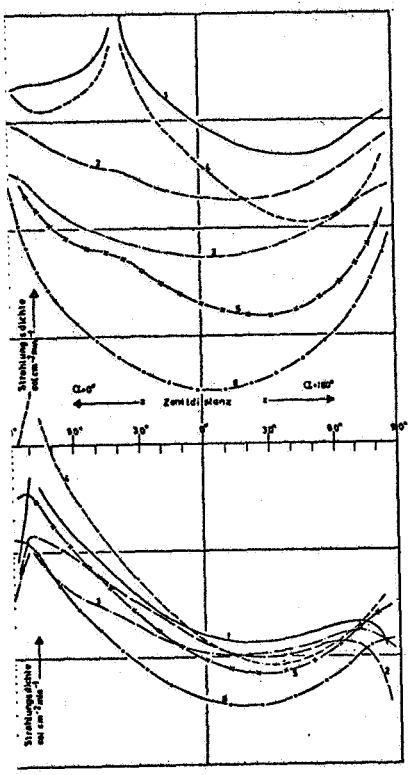

1 ——— λ = 0.45 μ, Einfachstreuung, primary scattering
2 – – – = 0.45 μ, Zweifachstreuung, secondary scattering
3 – · – · = 0.45 μ, Dreifachstreuung, third scattering
4 ----- = 0.85 μ, Einfachstreuung, primary scattering
5 – x – x = 0.85 μ, Zweifachstreuung, secondary scattering
6 – 0 – 0 = 0.85 μ, Dreifachstreuung, third scattering

Radiances in sun's vertical and sun's conter vertical. Zenith distance of the sun z_0 = 36.9°, turbidity factor T = 2.

1 ——— λ = 0.45 μ, Einfachstreuung, primary scattering
2 – – – = 0.45 μ, Zweifachstreuung, secondary scattering
3 – · – · = 0.45 μ, Dreifachstreuung, third scattering
4 ----- = 0.85 μ, Einfachstreuung, primary scattering
5 – x – x = 0.85 μ, Zweifachstreuung, secondary scattering
6 – 0 – 0 = 0.85 μ, Dreifachstreuung, third scattering

Radiances in sun's vertical and sun's conter vertical. Zenith distance of the sun z_0 = 78.5°, turbidity factor T = 6.

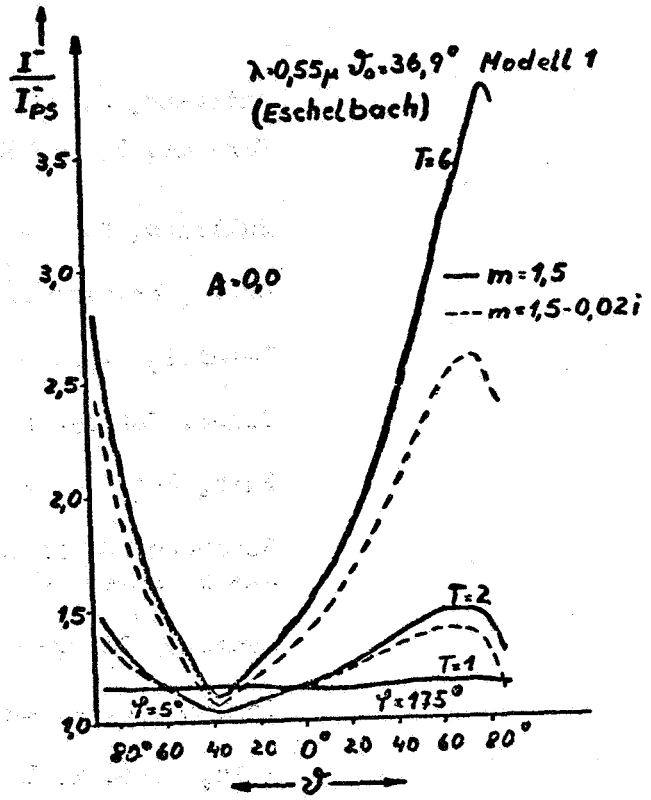

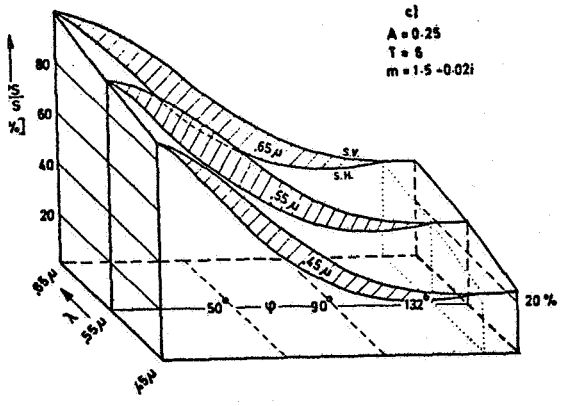

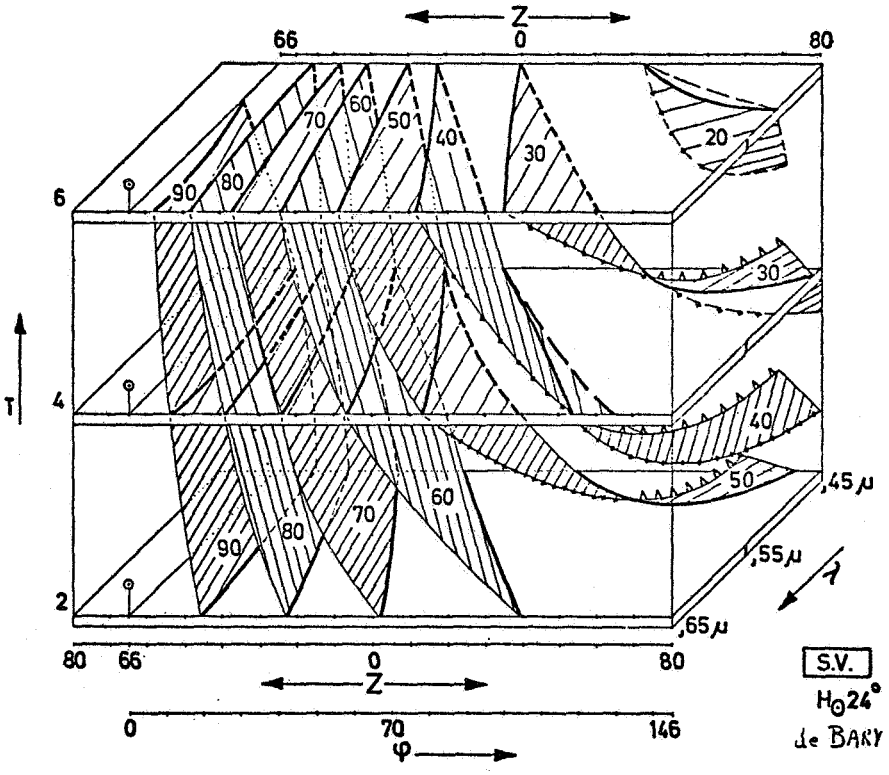

POST DEAD-LINE PAPERS

Key to Authors and Papers

Anderson, J. E. - PD5

Bary de, E, and K. Bullrich - PD7

Bullrich, K. - PD7

Chuan, Raymond L. - PD1

DeLuisi, J. J. - PD2

Jones, Carolyn F. - PD3

Park, Jae H. - PD3

Remsberg, Ellis E., Carolyn F. Jones, and Jae H. Park - PD3

Sverdup, George M. and Kenneth T. Whitby - PD4

Terhune, R. W. and J. E. Anderson - PD5

Volz, Frederic E. - PD6

Whitby, Kenneth T. - PD4

NASA-Langley, 1976